UNIMORE
UNIVERSITÀ DEGLI STUDI DI
MODENA E REGGIO EMILIA

UNIVERSITÀ DEGLI STUDI DI MODENA E REGGIO EMILIA

Dottorato di ricerca in
"Clinical and Experimental Medicine (CEM) – Medicina clinica e sperimentale"

Ciclo XXXVIII

New perspectives in the ophthalmological management of vitreoretinal lymphoma

Candidato: Dr. Pietro Gentile

Relatore (Tutor): Prof. Luca Cimino

Coordinatore del Corso di Dottorato: Prof. Marco Vinceti

ABSTRACT – PART 1

Anterior segment optical coherence tomography (AS-OCT) allows the exploration not only of the anterior chamber but also of the front part of the vitreous cavity. Our cross-sectional single-centre study investigated whether AS-OCT can distinguish between vitreous involvement due to vitreoretinal lymphoma (VRL) or vitritis in uveitis. We studied AS-OCT images from 28 patients (11 with biopsy-proven VRL and 17 with differential diagnosis uveitis) using publicly available radiomics software written in MATLAB. Patients were divided into two balanced groups: training and testing. Overall, 3260/3705 (88%) AS-OCT images met our defined quality criteria, making them eligible for analysis. We studied five different sets of grey-level samplings (16, 32, 64, 128, and 256 levels), finding that 128 grey levels performed the best. We selected the five most effective radiomic features ranked by the ability to predict the class (VRL or uveitis). We built a classification model using the xgboost Python function; through our model, 87% of eyes were correctly diagnosed as VRL or uveitis, regardless of exam technique or lens status. Areas under the receiver operating characteristic curves (AUC) in the 128 grey-level model were 0.95 [CI 0.94, 0.96] and 0.84 for training and testing datasets, respectively. This preliminary retrospective study highlights how AS-OCT can support ophthalmologists when there is clinical suspicion of VRL.

ABSTRACT – PART 2

The primary aim of the study was to explore the ability of a radiomics-based classification model to identify AS-OCT image features compatible with active VRL. The secondary aim was to investigate the possible association between the results of this non-invasive method and the aqueous tap molecular biomarkers currently used to determine VRL disease activity. We conducted a retrospective single-centre study of patients with biopsy-proven VRL, and at least one series of baseline or follow-up AS-OCT image scans and an aqueous tap. We extracted radiomic features from OCT images, five were selected and trained xgboost classifiers with leave-two-patients-out cross-validation (L2PO) to distinguish active (defined as the presence of lymphoma cells in anterior or vitreous chamber) from inactive disease (AUC as performance metric). If present, interleukin (IL)-10:IL-6 ratios were correlated with imaging features using logistic regression. Eight patients (22 visits total, 43 eyes) were analysed. From the L2PO analysis, we obtained an

AUC metric of 0.74 with a 95% confidence interval (CI) of 0.68–0.81. GLRLM_LRLGE was the feature most consistently associated with disease activity. When IL-10:IL-6 >1 was used as the outcome, the association weakened (all p-values >0.05), though mean and median values showed the same direction of effect. This pilot study explored the potential innovative role of radiomics to analyse VRL activity status using AS-OCT images. Although it is currently far from being a diagnostic tool, radiomic analysis could be the subject of future investigations aiming to refine non-invasive diagnostic strategies and treatment response assessment.

CONTENTS

1. INTRODUCTION (VITREORETINAL LYMPHOMA) 5

1.1 Epidemiology 5

1.2 Pathogenesis 5

1.3 Diagnosis 6

1.4 Treatment 11

1.5 Prognosis 12

1.6 Anterior Segment OCT (AS-OCT) and radiomics in VRL 13

1.7 A major challenge: the detection of VRL recurrence 14

1.8 Purposes 15

2. MATERIALS AND METHODS 15

2.1 Part 1 15

2.1.1 Image Acquisition 16

2.1.2 Imaging techniques 16

2.1.3 Radiomic analysis 16

2.1.4 Statistical analysis 18

2.2 Part 2 19

2.2.1 Imaging techniques 20

2.2.2 Radiomic analysis 20

2.2.3 Interleukins and mutation determinations 22

2.2.4 Statistical analysis 23

3. RESULTS 24

3.1 Part 1 24

3.2 Part 2 27

4. DISCUSSION 36

4.1 Part 1 36

4.2 Part 2 39

5. REFERENCES 43

1. INTRODUCTION (VITREORETINAL LYMPHOMA)

Vitreoretinal lymphoma (VRL) is defined as malignant lymphoproliferation involving the retina, the vitreous, and/or the optic nerve head. Primary VRL (PVRL) is regarded as a variant of primary central nervous system lymphoma (PCNSL) based on frequent synchronous or metachronous manifestations at both sites and similar clinical behaviour with rare dissemination outside of the central nervous system (CNS). The majority of PCNSL and 95% of VRL are classified as diffuse large B-cell lymphoma (DLBCL), which is also the most common non-Hodgkin lymphoma overall. Secondary VRL mostly occurs in the setting of PCNSL and is less frequent following systemic DLBCL, of which testicular lymphoma is the most common. PVRL is now recognized as the most frequent primary intraocular lymphoma.[1]

1.1 Epidemiology

The incidence is low, estimated at fewer than one case per million annually, yet its clinical impact is disproportionate given its masquerading presentation and high risk of CNS progression.[2] In the past three decades, the incidence of PCNSL appears to have tripled, as seen in the Finnish Cancer Registry and in the USA. It is not clear whether this observation is due to better diagnosis or an actual increase in numbers.[3]

Whereas PCSNL accounts for 4-6% of all brain tumors and <1% of all non-Hodgkin lymphomas, VRL is rare, constituting <0.01% of all ocular diseases.

At diagnosis, CNS involvement is present in 16-34% of VRL cases.[4] Between 50% and 90% of patients with VRL subsequently develop CNS disease (brain and/or spinal cord) within 16-24 months, while 15-20% of patients with PCNSL have concomitant VRL at presentation.[5,6]

VRL typically occurs in older individuals between 50 and 70 years of age, with a median age of 60 years. Regarding sex predilection, the data are conflicting.[1]

1.2 Pathogenesis

The etiology of VRL remains incompletely defined. A key unresolved question is whether lymphomatous cells enter the retina via retinal vessels, the optic nerve, or the choroid.

Two principal, non–mutually exclusive hypotheses have been advanced: an infectious model and a hematologic dissemination model.[7]

The infectious hypothesis posits that Epstein-Barr Virus (EBV) or Human Immunodeficiency Virus (HIV) infects lymphoid cells, triggering neoplastic transformation within the eye or the CNS. This view is supported by the frequent isolation of EBV in patients with acquired immunodeficiency syndrome (AIDS) and by the typically more aggressive clinical phenotype in this setting.[8]

The hematologic hypothesis emphasizes hematogenous spread of neoplastic lymphocytes from nodal or extranodal sites to the CNS and the eye.[9]

Given the association between VRL and PCNSL, lymphomatous cells may migrate along the optic nerve to reach the vitreous cavity, even though the optic nerve is only rarely involved clinically.[7]

1.3 Diagnosis

VRL is a real diagnostic challenge, often clinically mistaken for an inflammatory intraocular disease, and it is described as the most common uveitis masquerade syndrome. The insidious clinical presentation as chronic/recurrent uveitis, combined with the transient response to steroids, which are lymphocytolytic, causes a delay in diagnosis and appropriate treatment, often resulting in a poor prognosis with high mortality if CNS is involved.[10]

More than 80% of VRL patients have bilateral involvement, often asymmetrical.[11-13] Because anterior segment inflammation is usually minimal, conjunctival injection, pain, and photophobia are uncommon. Non-granulomatous keratic precipitates (KPs) may be scattered across the corneal endothelium and can assume a dendriform appearance in some cases. Occasionally, large aggregates of lymphoma cells on the endothelium mimic granulomatous KPs; corneal edema, pseudohypopyon, and pupillary distortion may occur, but are not frequent.[10]

In VRL, lymphoma cells infiltrate the vitreous body, the retina, or both.

Vitreous involvement occurs in the majority of patients affected by VRL. Clinically, vitreous cells can organize into sheet-like aggregates; compared with inflammatory vitritis, the cells tend to be larger but less dense, producing a “muddy” vitreous (Figure 1). Three vitreous haze patterns have been described: the “aurora borealis” pattern (46%),

a non-specific pattern (38%), and a “string-of-pearls” pattern (23%). The aurora borealis pattern—the most common—features opacification due to large lymphoma cells aligned in a radial, undulating fashion along peripheral vitreous fibrils (Figure 2).[14,15]

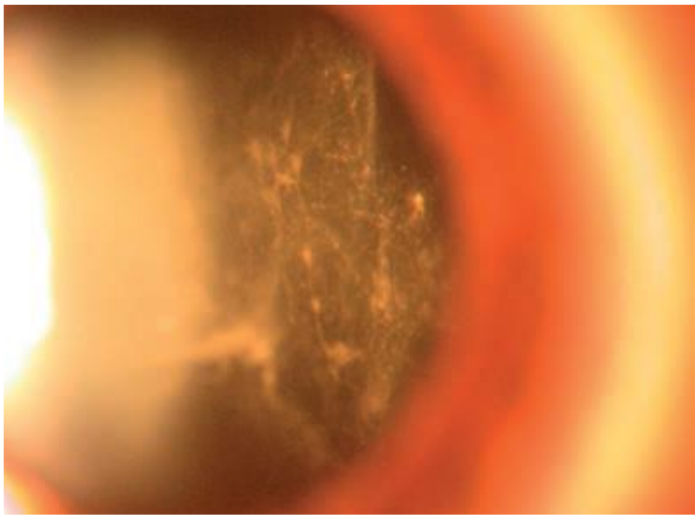

Figure 1. *Anterior vitreous of a patient with vitreoretinal lymphoma showing a “muddy” appearance, with sheet-like aggregates.*

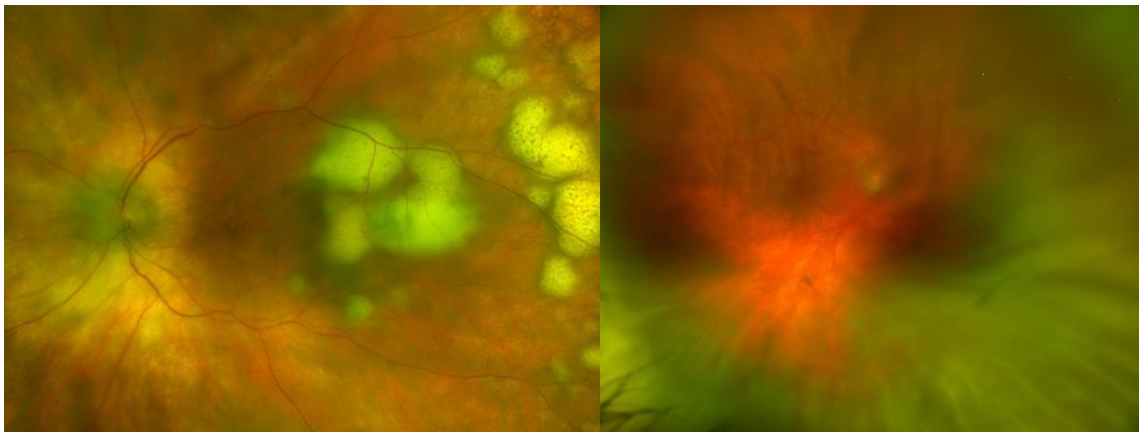

Figure 2. *Multifocal white-yellowish retinal lesions (left image) and vitreous aurora borealis pattern (right image).*

Multifocal white-yellow or cream-colored retinal or subretinal lesions strongly suggest VRL; migration of lymphoma cells beneath the retinal pigmented epithelium (RPE) and solid, irregular RPE detachments are considered pathognomonic (Figure 2). Such lesions occur in ~50% of cases and may cluster across the fundus, enlarge, or regress spontaneously, leaving RPE atrophy and subretinal fibrosis. Over time, retinal and subretinal lesions can develop a “leopard-skin” appearance in autofluorescence, due to

pigment deposition overlying prior foci. Other less common findings include necrotizing retinal infiltrates and retinal vasculitis.[16] In general, lymphoma cells can localize at any level of the retina, from the preretinal area to the sub-RPE (Figure 3).

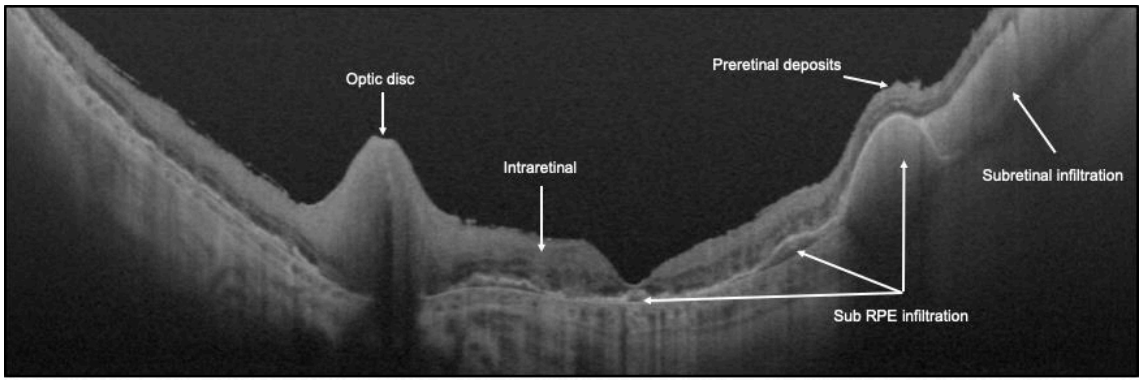

***Figure 3**. Optical coherence tomography image demonstrating infiltration of lymphomatous cells in several retinal areas.*

Diagnosing VRL is challenging and frequently delayed, with consequent increases in mortality and morbidity. Diagnostic confirmation of the clinical suspicion is required through examination of the vitreous fluid obtained by vitrectomy. The cytological analysis of vitreous fluid is considered the gold standard for PVRL diagnosis. However, a limited volume of vitreous sample, low numbers of lymphoma cells, poor cellular preservation, and degenerative changes caused by steroid use for presumed uveitis are the principal reasons for the rather variable (31–87.5%) and sometimes low diagnostic sensitivity of cytology alone. Various laboratory techniques have been employed to improve the diagnostic yield, including flow cytometry, immunocytochemistry, cytokine analyses, and molecular tests. Although diagnostic vitrectomy (pars plana) is conventional, anterior-chamber paracentesis is simpler, less invasive, and increasingly used with acceptable sensitivity—particularly for follow-up.[2]

Pars plana vitrectomy (PPV) is performed under local or general anesthesia. An undiluted ("dry") vitreous sample is most informative, but diluted cassette fluid should also be collected. Cutter rates of 600–1500 cuts/min (or lower) are recommended to optimize cell viability and diagnostic yield.[10]

Lymphoma cells are fragile and undergo morphologic degradation within ~60 minutes; therefore, samples must reach a pre-alerted pathology lab immediately for prompt processing. Alternatively, specimens may be placed in cell-preserving medium (e.g.,

bovine serum albumin) or a gentle cytologic fixative. Aqueous sampling is performed at the slit lamp under topical anesthesia using a 27- or 30-gauge needle. Retinal biopsy is rarely required.[17,18]

Because corticosteroids reduce activated lymphocytes in anterior chamber and vitreous, topical and systemic steroids should be stopped for at least two weeks before vitreous and/or aqueous sampling to improve diagnostic yield.[19]

Cytology remains the diagnostic gold standard. Sensitivity ranges from 31% to 87.5%, varying with cellularity and laboratory expertise. A positive cytology confirms lymphoma, whereas a negative result does not exclude it.[2,10] Malignant B cells are larger than benign lymphocytes, with scant basophilic cytoplasm; large, irregular, often clover-shaped hyper-segmented nuclei; coarse chromatin; and prominent nucleoli. Vitreous samples may also contain numerous reactive lymphocytes, cellular debris, and macrophages. Prior steroid therapy may induce degeneration and necrosis without compromising nucleic-acid integrity—still permitting molecular studies. Immuno-phenotyping can be performed by immunohistochemistry (IHC) or flow cytometry. A standard IHC panel identifies B cells (CD19, CD20, CD22, CD79a), T cells (CD2, CD3, CD4, CD5, CD7, CD8), NK cells (CD56), macrophages (CD68PG), and κ/λ light chains. Vitreous inflammation typically shows T-cell predominance, whereas VRL is marked by atypical B cells expressing CD20, PAX5, or CD79a, with macrophages and debris. Notably, statins can alter CD20 conformation and mask anti-CD20 binding; in such cases, anti-CD79a or anti-PAX5 antibodies should be used. Flow cytometry identifies target populations by antibody labelling and laser-based detection of scatter/fluorescence signals.[20,21]

During normal B-cell development, immunoglobulin (Ig) heavy- and light-chain genes undergo Variable, Diversity and Joining (V[D]J) recombination; each mature B cell produces a unique antigen-specific antibody. Polymerase chain reaction (PCR) targeting rearranged Ig genes yields a polyclonal smear in inflammatory samples but a discrete monoclonal product in neoplastic populations such as VRL. Determining B-cell clonality with IgH and Igκ primers is a valuable diagnostic adjunct on vitreous samples; reported sensitivity averages 46–95%, influenced by primer choice. Because VRL frequently harbors extensive somatic hypermutation that impairs primer binding, false-negatives may occur even with optimal cellularity and technique. Conversely, ocular immune

privilege can favor oligoclonal/monoclonal expansions of non-neoplastic lymphoid cells, generating false positives.[22-27]

About two decades ago, Chan et al. reported elevated IL-10 in vitreous from VRL and elevated IL-6 in uveitis; an IL-10/IL-6 ratio >1 favored lymphoma (sensitivity ~92%).[28] IL-10 functions as a growth factor for malignant B cells, whereas IL-6 is an inflammatory cytokine typical of uveitis. Subsequent studies have shown the IL-10/IL-6 ratio is informative in aqueous humor as well; combining aqueous and vitreous testing improves accuracy. Nonetheless, no universal IL-10 cutoff exists due to a diagnostic "gray zone" and a ratio <1 does not reliably exclude VRL.[29]

To address these limitations, the Hôpital Pitié-Salpêtrière group developed the Interleukin Score for IntraOcular Lymphoma Diagnosis (ISOLD), which estimates the probability of intraocular lymphoma (i-IOL) from IL-10 and IL-6 levels in aqueous or vitreous:

• Aqueous ISOLD: $-12.871 + 5.533 \times \log(\text{IL-10} + 1) - 1.614 \times \log(\text{IL-6} + 1)$

• Vitreous ISOLD: $-12.208 + 4.648 \times \log(\text{IL-10} + 1) - 1.669 \times \log(\text{IL-6} + 1)$

The posterior probability of i-IOL = $1 / (1 + \exp[-\text{ISOLD}])$. Patients are stratified as:

-Certainly not i-IOL: ISOLD < −4.6 (posterior probability ≪ 1%);

-Probably not i-IOL: −4.6 < ISOLD < 0;

-Probably i-IOL: 0 < ISOLD < +4.6;

-Certainly i-IOL: ISOLD > +4.6 (posterior probability ≫ 99%)(104).

This score mitigates the IL-10/IL-6 ratio's discordance, offering high sensitivity and specificity for B-cell VRL.[30]

In VRL, MYD88 mutations are frequent (~70% in vitreous samples), implicating Toll-like receptor signaling; CD79B and other B-cell-receptor pathway genes are also commonly mutated. Cani et al. reported MYD88 gain-of-function mutations (L265P, S243N) that constitutively activate NF-κB, a potential target of ibrutinib, a Bruton tyrosine kinase inhibitor. MYD88 assays have been developed for aqueous humor as well. A pilot study suggests that combining cytology, IgH clonality testing, and MYD88 mutation analysis yields high diagnostic accuracy.[31,32]

1.4 Treatment

The therapeutic goal in PVRL is twofold: eradication of intraocular disease and prevention of CNS dissemination. Optimal management of VRL requires a multidisciplinary approach involving Ophthalmology, Oncology, Hematology, Neurology, and Radiology.

Intravitreal methotrexate (MTX) is effective in inducing clinical remission in isolated primary VRL and in VRL secondary to PCNSL. In 2002, Smith et al. proposed an intravitreal chemotherapy protocol for PCNSL with ocular involvement: an induction phase of two injections per week for one month, using 400 μg/0.1 mL injected via the pars plana with a 30-gauge needle; a consolidation phase of one injection weekly for two months; and maintenance of one injection monthly for nine months. MTX induced VRL remission under this regimen. In 2008, Frenkel et al. reported outcomes in 44 eyes (26 patients) treated with intravitreal MTX 400 μg/0.1 mL: twice weekly for 4 weeks, then weekly for 8 weeks, and finally monthly for 9 months (total 25 injections). Clinical remission was achieved after a mean of 6.4 injections.[33-35]

Rituximab (RTX), an anti-CD20 monoclonal antibody, has been administered intravitreally for the treatment of CD20-positive VRL. A typical regimen is 1 mg/0.1 mL weekly for four weeks; approximately half of the patients relapse. Nevertheless, RTX may be a reasonable alternative to MTX given its lower ocular toxicity profile.[36]

Ocular radiotherapy remains in use for isolated VRL: doses of 30–45 Gy in 15 fractions can achieve complete remission. For patients with concomitant CNS disease who are refractory to systemic chemotherapy and are not candidates for more aggressive therapy, combined ocular and whole-brain irradiation can be a viable option. Risks of ocular radiotherapy include radiation retinopathy, optic atrophy, cataract, and dry eye; cranial irradiation carries risks of neurotoxicity, ataxia, cognitive decline, and even death. The field continues to debate whether ocular radiotherapy or intravitreal chemotherapy should be considered first-line.[37]

A persistent question is whether prophylactic systemic chemotherapy prevents CNS involvement or prolongs CNS progression-free survival. Retrospective and prospective studies have yielded mixed results regarding overall survival benefits. Two retrospective series found systemic chemotherapy did not prevent CNS spread. Conversely, other studies support a prophylactic benefit in preventing or delaying CNS involvement.[38-42]

Although no single systemic regimen is standard, high-dose intravenous MTX is generally considered first-line for VRL with CNS disease, avoiding orbital irradiation-related ocular toxicity. MTX induces remission in up to 72% as monotherapy and 94–100% in combination regimens; median survival improved from 28 to 85 months with high-dose systemic chemotherapy. High-dose thiotepa, busulfan, and cyclophosphamide followed by autologous peripheral blood stem-cell transplantation is reserved for poor responders or relapsed disease. The IELSG32 trial provided high-level evidence supporting MATRIx (MTX, cytarabine, thiotepa, RTX) as a standard for PCNSL patients ≤70 years. At 30 months, complete remission was 49% with MATRIx versus 23% with MTX–cytarabine and 30% with MTX–cytarabine–RTX.[38-42]

Overall, because VRL is rare and treatment protocols vary, the literature does not clearly demonstrate that systemic therapy prevents CNS involvement in VRL. A large, international multicenter study is needed to define the optimal regimen.

1.5 Prognosis

Diagnosis of VRL is frequently delayed: on average, ~12 months elapse from symptom onset to diagnosis, and symptoms can precede diagnostic consideration by 2–3 years. Contributing factors include its masquerade as nonspecific intermediate/posterior chronic uveitis; relatively preserved visual acuity despite vitritis/floaters; and an initial corticosteroid response followed by steroid-dependence or refractoriness to immunosuppression.[2]

Mortality data are heterogeneous due to small cohorts, variable treatments, and limited follow-up. Reported mortality ranges 9–18% over 12–35 months of follow-up. Five-year overall survival is <25%, underscoring the poor prognosis. In a multicenter study across 16 centers in 7 countries, overall survival and progression-free survival were 31 and 18 months, respectively; local ocular therapy controlled intraocular disease but did not improve survival.[10]

Some authors argue that, in isolated ocular disease, early systemic therapy—before CNS involvement—is associated with better survival and, while not preventing CNS spread, may delay it. Others report that combined local and systemic chemotherapy improves progression-free survival but not overall survival, or prevents CNS involvement without significantly improving overall survival.[43-46]

Isolated VRL carries a better survival than VRL with CNS disease. Among patients who develop PCNSL, 24–40% have an overall survival of about 1 year. On average, ~3 months separate initial CNS symptoms from the diagnosis of CNS lymphoma. Thus, CNS involvement is a negative prognostic factor, and sub-RPE infiltrates have also been associated with reduced survival.[43-46]

1.6 Anterior Segment OCT (AS-OCT) and radiomics in VRL

A key feature of VRL is the vitreous involvement represented by a characteristic infiltration due to the invasion of lymphoma cells that form sheets or strands with vitreous turbidity. This is evident during the ophthalmological examination when carefully looking at the anterior vitreous. However, because this feature is difficult to recognise, it enters the differential diagnosis with the uveitis that causes significant vitreous haze.

As such, the possibility of imaging and objectively evaluating the anterior vitreous with AS-OCT would be a significant added value for the differentiation between vitreous haze, making it possible to detect a particular potential pattern in VRL, and could be an important ancillary test in its diagnosis.

AS-OCT is a fast, easy, and non-invasive imaging technique that has recently gained prominence in the description of inflammatory changes in the anterior vitreous of patients with uveitis. Zicarelli et al. were able to obtain OCT images of the anterior vitreous in the area just behind the lens, which had previously been inaccessible to this imaging technique due to its location, too forward for the posterior segment and too far back for anterior segment OCT. These authors pushed the device towards the eye being studied and disabled the tracking, thus not following the recommendations on its use. As a result, the cornea was flipped onto the lens, which was in the upper part of the image, and the structures behind it could be seen in the lower part of the scan.[47]

AS-OCT has proved to be useful to identify cells with high-resolution brightness scans (B-scan) and to indirectly quantify anterior chamber flare, thus contributing to a more objective assessment of intraocular inflammation in patients with uveitis. Likewise, posterior segment OCT provides high-resolution imaging that correlates well with the clinical grading of vitreous haze, and may offer indirect evidence of disease activity in VRL.[48-50]

Radiomics is a novel methodology in precision medicine that employs well-defined mathematical formulas to describe medical images quantitatively. This approach is an application of artificial intelligence (AI) that calculates features directly from the images' pixel values or filtered versions of the original captures. The mathematical formulas express the distribution and relationships between pixels and voxels within a specific region of interest (ROI) in the images. Within a biomedical image, there are complex details that may be beyond the human eye's perception; this is what radiomics is based on. Radiomic features are numerical descriptors that enable a non-invasive exploration of potential correlations between the information derived from the images acquired during the routine clinical pathway of the patient and the clinical or biological features seen on the images.[49]

1.7 A major challenge: the detection of VRL recurrence

The diagnosis of a post-treatment recurrence of VRL remains challenging. This is due to the inherent limitations of clinical evaluation alone in definitely diagnosing relapses, as well as the lack of standardized international guidelines to support the ophthalmologist in identifying suspected recurrences. To date, there are no universally accepted objective parameters to quantify treatment response or detect any relapse in terms of tumor cell infiltration into the vitreous and/or retina. Standard clinical ocular examination does not always prove to be decisive in this sense. In cases where VRL recurrence is suspected, an anterior chamber paracentesis is generally considered to be easier and more repeatable compared to vitrectomy. This technique allows for the collection of a small amount of aqueous humour, enabling the same molecular investigations carried out on vitreous samples during the initial diagnostic workup. These encompass the quantification of IL-10 and IL-6, detection of IgH gene rearrangements, and identification of the MYD88 mutation, which is commonly associated with VRL.[10]

Currently, a few reports have described the use of IL-10, IL-6 and their ratio and of MYD88 in the aqueous humour for monitoring the therapeutic response. Moreover, while aqueous tap is considered a minimally invasive procedure, it nonetheless remains a surgical intervention that might expose the patient to intra- and post-operative risks, such as infection, hypotony, or anterior chamber trauma. Therefore, the development of a non-

invasive test would represent a useful diagnostic tool in the management of patients affected by VRL.[52,53]

Nowadays, there is no validated imaging modality for the non-invasive detection of VRL recurrence.

1.8 Purposes

The first part of this thesis aims to investigate the ability of radiomic features to perform a differential diagnosis of the vitreous (VRL vs uveitis) using AS-OCT imaging.

Whereas the purpose of the second part is to evaluate the possible role of AS-OCT in the identification of VRL relapse. This design is built by carrying out a correlation with the results obtained in laboratory findings from aqueous humour samples (including IL-6 and IL-10 quantification, MYD88 sequencing, and IgH rearrangements).

In order to achieve our goal in both parts, we tried to develop a radiomics-based classification model capable of identifying AS-OCT image features compatible with VRL diagnosis (first section) and relapse (second section).

The considered classification models could represent the foundation for the development of an AI-driven diagnostic software platform capable of obviating the need for invasive procedures in the diagnosis of VRL or its recurrence and providing a non-invasive tool available to ophthalmologists in clinical practice.

2. MATERIALS AND METHODS

2.1 Part 1

We analysed patients evaluated at the Ocular Immunology Unit of the AUSL-IRCCS of Reggio Emilia (Italy) between January 2019 and December 2022; we considered biopsy-proven VRL and uveitis characterised by anterior vitritis, such as Fuchs uveitis, sarcoidosis uveitis, Behçet uveitis and uveitis of unknown origin, in differential diagnosis with VRL. We named the latter group “vitritis”. The study was conducted in agreement with the principles of the Declaration of Helsinki and received approval from the local

ethics committee (protocol n. 2019/0085664 Comitato Etico dell'Area Vasta Emilia Nord, Italy).

2.1.1 Image Acquisition

The images were obtained with swept-source AS-OCT ANTERION (Heidelberg Engineering, Heidelberg, Germany), which offers an improved signal penetration (wavelength 1300 nm), a very high resolution (axial and transverse resolution in tissue <10 µm and 30 µm, respectively), and an enhanced depth of scan (14 ± 0.5 mm). Before May 2022, the acquisitions were performed using the recommended acquisition settings of the OCT device (referred to here on as "old"). Conversely, the new acquisition technique described above will be referred to as "new".[47]

2.1.2 Imaging techniques

We extracted anonymised Digital Imaging and Communications in Medicine (DICOM) images directly from the OCT system. Next, two experienced ophthalmologists manually segmented the vitreous area in the images from the sub-lens region up to the end of the visible vitreous using a rectangular-shaped ROI as shown in Figure 4. The area of these ROIs depended on several variables, particularly the exam technique, the anatomical localisation of the slice, and the patient's individual clinical conditions. We performed exams with the "old" and the "new" method of pushing the device forward, the latter one for patients referred after May 2022. Image width depended on the relative distance from the optical axis, and the length relied on the exam technique. If the selected area was less than 13,500 pixels, we did not include its respective images in our analysis according to similar results found for the radiomics predictive model applied in oncology.[54] In addition, we rejected slices with artefacts caused by the hyper-reflective bend zone generated by the cornea shadow on the anterior vitreous cavity, as mentioned above.

2.1.3 Radiomic analysis

We used the Radiomics tool (Version 1.2.0.0 by Martin Vallières, publicly available at https://it.mathworks.com/matlabcentral/fileexchange/51948-radiomics, accessed on 5 July 2023) to extract radiomic features with the aforementioned image segmentations as

inputs.[55] Radiomics software is a free program running on MATLAB® (Mathworks, Natick, MA, USA). We used MATLAB version R2021b. This software was designed to calculate 43 features: three from the image histogram (variance, skewness, and kurtosis), nine from the Gray-Level Co-Occurrence Matrix (GLCM), 13 from the Gray-Level Run-Length Matrix (GLRLM), 13 from the Gray-Level Size Zone Matrix (GLSZM) and five from the Neighborhood Gray-Tone Difference Matrix (NGTDM).[55-57]

It is worth noting the meaning of the radiomic features selected to build the discriminant model. GLRLM_LRHGE quantifies grey-level runs (i.e., the number of consecutive pixels having the same grey-level value). GLCM_Correlation shows the linear dependency of grey-level values on their respective pixels in the grey-level co-occurrence matrix (0 = perfect decorrelation, 1 = ideal correlation). NGTDM_Coarseness measures the average difference between the central pixel's grey level and that of its neighbour; this is an indicator of the spatial rate of grey-level variation. A higher value means a lower spatial change rate and a locally more uniform texture. NGTDM_Strength measures the primitive shapes in the image (i.e., the presence of simple elements such as arcs, squares, or other simple shapes in the image). A higher value means the primitives are easily defined and visible; it also means a slow change in intensity but a larger coarse difference in grey-level tones. GLSZM_HGZE quantifies the distribution of the higher grey-level-connected pixels that share the same grey-level intensity. A higher value indicates a greater proportion of higher grey-level tones and size zones in the image. GLRLM_SRE measures the distribution of short run lengths. A higher value indicates shorter run lengths and more refined texture. NGTDM_complexity describes the presence of many primitive components in the image; it also measures the image's non-uniformity and rapid changes in grey-level intensity.[55-57]

Before feature extraction from 2D images, we used the following pre-processing parameters: the number of grey levels (Ng = 16, 32, 64, 128, 256), equal quantisation (i.e., the ROI was equalised to increase the contrast), isotropic pixel size (8.843 μm), and 'scanType' equal to 'Other'; no wavelet band-pass filtering was performed. The patients were preliminarily divided into two groups: training and testing. The first set was composed of 14 patients (seven vitritis—11 eyes—53% images of the training dataset, and seven VRLs—11 eyes—47% images), as well as the second one (10 vitritis—17 eyes—68% images of the testing dataset, and four VRLs—eight eyes—32% images). The

dataset had a good balance in the training group in terms of acquisition method, lens type, and outcome. The first step in the analysis consisted of feature scaling using Scikit learn.[58]

2.1.4 Statistical analysis

The correlation between the variables was studied using the Pearson correlation coefficient (r) for radiomic models built with five different sets of grey-level sampling (16, 32, 64, 128, and 256 levels).

Within the training dataset, five features were selected for each model using the xgboost Python function; the features were selected using feature importance greater than 0.03. Then five models were built using the xgboost algorithm using early stopping round equal to 100 and a learning rate equal to 0.01. The areas under the receiver operating characteristic curves (AUCs) were calculated with their confidence interval for the training dataset using bootstrapping methods (500 repetitions were performed). In addition, the accuracy and precision were calculated for training and testing sets.

The models assigned to each image have the probability of belonging to the VRL class. If this probability was less than 0.5, the image was classified as belonging to the vitritis group, as the outcome was binary. Each eye was assigned to a group based on whether the majority of that eye's images were classified as VRL or as vitritis.

Clinical features considered in the statistical analysis were age at diagnosis (years), sex, laterality, lens status (phakic or pseudophakic), and acquisition method (old and/ or new).

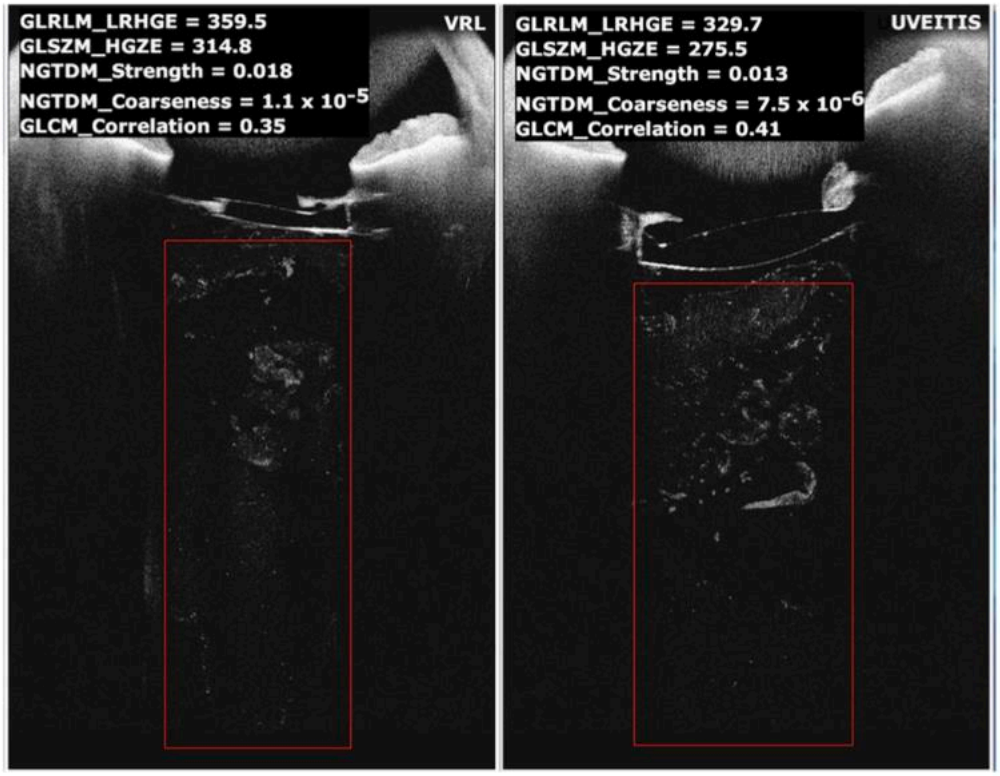

Figure 4. *Comparison of two images: one patient with vitreous involvement in VRL (left) and one with vitritis (right). The rectangular-shaped ROI shows the area where the software calculated the radiomic features. In the upper left are shown, for example, the numerical value of the features used by the model built using 128 grey levels.*

2.2 Part 2

We retrospectively analysed patients examined at the Ocular Immunology Unit of the AUSL-IRCCS of Reggio Emilia (Italy) between February 2022 and April 2024 who had received a biopsy-proven diagnosis of VRL and had had at least one series of AS-OCT image scans and an aqueous tap. All patients routinely underwent OCT in both eyes, while an aqueous tap was performed only in the eye where there was greater suspicion of active VRL as it is an invasive procedure. The study was conducted in agreement with the tenets of the Declaration of Helsinki and received approval from the local ethics committee (protocol n. 2019/0085664, Comitato Etico dell'Area Vasta Emilia Nord, Italy, and

subsequent substantial amendments, last approved on October 2025, with protocol n. 2025/0136790).

2.2.1 Imaging techniques

AS-OCT imaging was performed at baseline (i.e., prior to treatment initiation) whenever possible, and at least every 12–15 months thereafter, or earlier in cases of clinical worsening, in conjunction with a diagnostic aqueous tap, to identify relapses.

The main clinical outcome was active disease, defined as the presence of lymphoma cells in the anterior chamber, vitreous cavity, or retina. The complement outcome was inactive disease, defined as the absence of any evidence of residual disease within the anterior chamber, vitreous cavity, or retina.[59,60]

We acquired AS-OCT images with ANTERION (Heidelberg Engineering, Heidelberg, Germany). This swept-source OCT device operates at a 1300 nm wavelength to enhance tissue penetration, provides in-tissue axial and transverse resolutions of <10 µm and ~30 µm, respectively, and supports scan lengths of 14 ± 0.5 mm. We obtained OCT images of the anterior vitreous by pushing the device towards the eye being studied. Because no tracking solution is available to ensure identical positioning within the anterior vitreous, we predefined a reproducible acquisition zone behind the lens up to the end of the visible vitreous. For each eye, we collected one or more series of 25 horizontal B-scans, each 14 mm in length, spanning a total vertical extent of 6 mm, with a nominal sampling resolution of 13.69 µm.

2.2.2 Radiomic analysis

Anonymized Digital Imaging and Communications in Medicine (DICOM) files were exported directly from the AS-OCT system. All images underwent quality control; scans with evident artefacts, most notably the hyper-reflective bending area caused by corneal shadowing in the anterior vitreous, were removed. Two experienced ophthalmologists manually delineated the vitreous using rectangular ROIs extending from sub-lenticular region to the most posterior extent of visible vitreous (Figure 5). ROI size varied according to acquisition technique, slice location, and patient-specific clinical factors; the image width depended on the relative distance from the optical axis. ROIs with a pixel

count <13,500 were excluded, consistent with thresholds reported for radiomics-based predictive modelling in oncology.[61]

After confirming image quality, we extracted radiomic features with the Radiomics tool (version 1.2.0.0) using the segmented ROIs as input. The software is available free of charge and is implemented in MATLAB® (MathWorks, Natick, MA, USA); all analyses were performed in MATLAB R2021b. Each image went through a classification algorithm that determined its probability of being assigned to the "inactive" or the "active" disease category. A binary threshold of 0.5 was applied: if the cited probability was less than 0.5, the image was classified as belonging to the inactive group. Each eye was assigned to a group based on whether the majority of its images were classified as active or inactive disease.

Using radiomics MATLAB software, we extracted a total of 43 features from each image segmentation: histogram distribution (n=3), GLCM (n=9), GLRLM (n=13), GLSZM (n=13) and NGTDM (n=5). Our radiomics pipeline consisted of the following steps: i) removal of correlated features (those with a Pearson's r^2 greater than 0.75); ii) splitting into training and testing sets; iii) estimation of the optimal XGBoost parameters; iv) fitting the XGBoost weights to the training and validation (obtained in a subsequent splitting of the training set) data; v) evaluation of the model performance on the testing set; vi) model's explainability. The splitting into training and testing sets was performed using patient information, ensuring that images of the same patient were not present in both the training/validation and testing sets. Due to the low number of patients, we addressed a possible bias in the splitting phase by using a cross-validation strategy consisting of studying all possible combinations of models, leaving two patients out (L2PO).[62,63] The rationale for this was to choose a fair combination that could describe the potential information of this method, preventing both too optimistic and overly pessimistic scenarios. For every cluster, we selected the best features using the XGBoost algorithm.

The primary performance metric was the area under the ROC curve computed by using images from the two patients left out in each combination (the so-called out-of-bag patients). To estimate the uncertainties, we used a cluster-aware bootstrap on the testing set (within the same patient we sampled using the cluster structure), and a 95% confidence interval (95% CI) was calculated. For each cluster, we calculated the area under the curve

(AUC) on the training and testing sets to compute the overall performance score (see Eq. 1):

$$score = AUC_{train} - AUC_{test} \qquad Eq.\ 1$$

Regarding the model's explainability, we used SHapley Additive exPlanations (SHAP) to quantify the contribution of each selected radiomic feature to the XGBoost model's predictions. For each subject, SHAP provides feature-level attributions relative to a baseline (expected model output), with additive consistency: the baseline plus the sum of SHAP values equals the model output. Global feature importance was summarized by aggregating absolute SHAP values across subjects.[64-66]

The radiomic model pipeline was executed with an in-house Python script.

2.2.3 Interleukins and mutation determinations

Concentrations of IL-6 and IL-10 in AH samples were measured using the Elecsys IL-6 immunoassay (IVD, Cobas), purchased from Roche, and the IL-10 solid phase enzyme amplified sensitivity immunoassay (REF: EIA-4699, IVD), purchased from DRG Instruments. The lower limits of detection of IL-6 and IL-10 were, respectively, 1.5 pg/ml and 1.6 pg/ml. Both assays have been validated by the manufacturers on serum samples, and the IL-6 kit also on plasma samples. References ranges are thus available only for serum and plasma samples (0-7 pg/ml for IL-6; 0-3.3 pg/ml for IL-10). The samples were always tested at multiple dilutions (1:10, 1:20, 1:40) to verify the linearity of the analytical data. An IL-10:IL-6 ratio >1 is suggestive of active disease.

Regarding MYD88, PlentiPlex™ MYD88 L265P assay (PentaBase ApS Lumbyvej 19G 5000 Odense C, Denmark) was designed to detect the leucine-to-proline mutation in codon 265 of the Myeloid differentiation primary response 88 protein (MYD88 L265P) in genomic DNA (gDNA) samples. The test can detect the presence of the L265P mutation, constituting up to 0.25% of a human gDNA sample (from formalin-fixed paraffin-embedded tumour biopsies).

Regarding clonality B, the test is on the rearrangement of the IgH: FR1-JH, FR2-JH and FR3-JH regions. It is a clonality search through PCR reactions, which are then run on the sequencer with an analysis of fragments in capillary electrophoresis.

2.2.4 Statistical analysis

Summary measures (mean, median, standard deviation, 10th and 90th percentiles) were calculated for each feature based on data collapsed at the individual-visit-eye level.

Univariate logistic regression models were built to assess the association between each summary measure and the two determinable outcomes: clinical and molecular. Results are reported as odds ratios (ORs) with 95% confidence intervals (CIs).

Logistic regression models were used to evaluate the association between individual radiomic features extracted from AS-OCT images and clinical outcome (inactive vs active disease) using five different distributional summaries: mean, median, standard deviation and 10th and 90th percentiles. Analyses were conducted on a per-visit level, accounting for within-subject correlation using the svy command in Stata/SE version 18 to obtain robust standard errors in the logistic regression models.

To visualize the relationship between molecular outcome and feature summaries, we considered only the cytokine balance and plotted the IL-10:IL-6 ratio against the synthetic summary measures of the features, grouped by clinical outcome. We did not consider in the statistical analysis the MYD88 L265P mutation and the IgH rearrangements as molecular outcomes because the number of available data were too low.

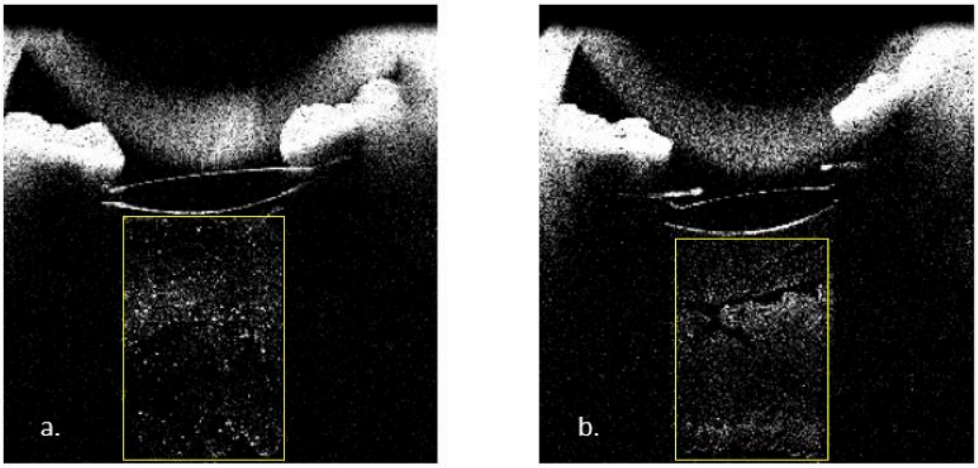

Figure 5*. Comparison of two anterior segment optical coherence tomography (AS-OCT) images during follow-up: one patient with active (a) and one with inactive (b) VRL disease. The yellow rectangular-shaped region of interest (ROI) shows the area where MATLAB software calculated the radiomic features.*

3. RESULTS

3.1 Part 1

Eleven patients with biopsy-proven VRL (a total of 19 eyes) and 17 patients (a total of 28 eyes) with vitritis were included in this retrospective study. Specifically, five patients with Fuchs uveitis, four patients with sarcoidosis uveitis, two patients with Behçet uveitis, and six patients with uveitis of uncertain origin were enrolled in the group of vitritis. Clinical features are summarised in Table 1. In both groups, there were more bilateral than unilateral cases, and unilateral uveitis were Fuchs uveitis or uveitis of uncertain origin. A total of 31 eyes were phakic and 16 were pseudophakic. There were 13 males and 15 females. The mean age of vitritis patients was 55 years old (20–79), while that of VRL patients was 72 (51–94) years old.

Overall, 3260/3705 (88%) AS-OCT images met our defined quality criteria, making them eligible for analysis. Specifically, 2131 images were from eyes of patients with uveitis, while 1129 were from eyes of patients with biopsy-proven VRL.

Table 2 shows the patient stratification per eye site, acquisition method, lens type, and sex.

Age, sex, lens type (phakic or pseudophakic) and eye site (left or right) did not demonstrate any correlation with the outcome ($r = 0.4$, $r = 0.1$, $r = 0.1$, and $r = 0.0$, respectively). We observed a moderate correlation ($r = 0.5$) between vitritis outcome and acquisition method that was intrinsically dependent on the ROI area.

Table 3 reports the models' results for the different sets of grey-level sampling considered in the radiomic analysis pre-processing. The model using 128 grey levels (Dataset Ng = 128) demonstrated the best performance in terms of AUC in both the training and the testing dataset, 0.95 [CI 0.94, 0.96] and 0.84, respectively; in this model, accuracy was 0.860 and 0.781 in the training and the testing dataset, respectively, and precision was 0.985 and 0.582 in the training and the testing dataset, respectively. Using this model, 41/47 (87%) of eyes corresponding to 23/28 (82%) of patients were correctly diagnosed as VRL or uveitis, regardless of the exam technique used or lens status. We clarify that we have considered a patient as correctly classified only if both eyes were properly identified in case of bilateral involvement. The ROC curves relative to the 128 gray level

model is shown in Figure 6. Table 4 gathers the Pearson correlation coefficients among the radiomic features employed in the 128 grey-level model since the latter is the one that proved to perform the best.

Patient Code	Patient Sex	Analyzed Images (n)	Label	Site	Age (y)	Acquisition Method	Training	Testing	Lens Type Left Eye (L)	Lens Type Right Eye (R)
433	F	124	Vitritis (FU)	R,L	26	both	X		Phakic	Phakic
434	M	98	Vitritis (OS)	R,L	57	new	X		Phakic	Phakic
439	F	132	Vitritis (OS)	R,L	74	new	X		Phakic	Phakic
440	M	99	Vitritis (FU)	L	50	new	X		Phakic	N.A.
444	M	97	Vitritis (FU)	L	39	new	X		Phakic	N.A.
445	M	114	Vitritis (OS)	R,L	52	new		X	Pseudo-phakic	Pseudo-phakic
405	M	111	Vitritis (FU)	R	38	old	X		N.A.	Phakic
435	F	96	Vitritis (BU)	R,L	20	new	X		Phakic	Phakic
437	F	239	Vitritis (BU)	R,L	26	new		X	Phakic	Phakic
438	M	95	Vitritis (OS)	R,L	46	new		X	Pseudo-phakic	Pseudo-phakic
448	F	217	Vitritis (FU)	R,L	65	old		X	Phakic	Phakic
410	F	109	Vitritis (UUO)	R,L	79	old		X	Pseudo-phakic	Pseudo-phakic
446	F	110	Vitritis (UUO)	L	66	both		X	Phakic	N.A.
466	F	90	Vitritis (UUO)	R	62	both		X	N.A.	Phakic
468	F	124	Vitritis (UUO)	R,L	78	both		X	Pseudo-phakic	Pseudo-phakic
491	M	174	Vitritis (UUO)	R,L	75	both		X	Pseudo-phakic	Pseudo-phakic
493	F	102	Vitritis (UUO)	L	79	both		X	Pseudo-phakic	N.A.
393	F	56	VRL	R,L	91	New	X		Pseudo-phakic	Pseudo-phakic
432	M	132	VRL	R,L	73	new		X	Phakic	Phakic
436	M	166	VRL	R,L	76	new	X		Pseudo-phakic	Phakic
442	F	62	VRL	R,L	88	new	X		Phakic	Pseudo-phakic
447	M	95	VRL	R	99	new	X		N.A.	Pseudo-phakic
103	M	82	VRL	R,L	55	old		X	Phakic	Phakic
173	M	145	VRL	R,L	51	old	X		Phakic	Phakic
186	M	18	VRL	L	58	old	X		Phakic	N.A.
363	F	80	VRL	R,L	71	old		X	Phakic	Phakic
364	F	32	VRL	L	82	old	X		N.A.	Phakic
398	F	261	VRL	R,L	58	old		X	Phakic	Phakic

Table 1. *Database representation showing the patient selection and images number used for training and testing groups. The lens description per each eye site is also reported (L: left or R: right). F: female; M: male; N.A.: not acquired; FU: Fuchs uveitis; OS: ocular sarcoidosis; BU: Behçet uveitis; UUO: uveitis of uncertain origin.*

	Site															
	L Acquisition Method								R Acquisition Method							
	New Lens Type				Old Lens Type				New Lens Type				Old Lens Type			
	Phakic Sex		Pseudo-Phakic Sex		Phakic Sex		Pseudo-Phakic Sex		Phakic Sex		Pseudo-Phakic Sex		Phakic Sex		Pseudo-Phakic Sex	
	M	F	M	F	M	F	M	F	M	F	M	F	M	F	M	F
Vitritis (n)	247	326	161	44	0	40	19	98	47	432	172	27	111	113	31	64
Average age (y)	47.1	46.3	63.8	78	NA	41.9	78	79	57	45.4	59	78	38	46.7	66	79
VRL (n)	44	37	94	0	129	191	23	39	137	0	95	25	116	182	0	17
Average age (y)	73	88	76	NA	53.2	61.3	76	91	74.1	NA	94	88	52.4	64.5	NA	91

Table 2. *Patients' stratification per eye site, acquisition method, lens type, and sex. n: number of images for each class; y: years; L: left; R: right; M: male; F: female; N.A.: not acquired.*

	Accuracy (Train) (Test)	Precision (Train) (Test)	AUC (Train [CI 95%]) (Test)	Radiomic Features Selected
Dataset Ng = 16	0.878 0.735	0.968 0.525	0.947 [0.937–0.956] 0.813	GLCM_Homogeneity, NGTDM_Busyness, GLRLM_LRHGE, NGTDM_Coarseness, GLCM_Correlation
Dataset Ng = 32	0.844 0.825	0.987 0.790	0.938 [0.928–0.949] 0.798	GLRLM_LRHGE, GLCM_Contrast, NGTDM_Coarseness, GLCM_Correlation, GLCM_Homogeneity
Dataset Ng = 64	0.860 0.827	0.995 0.798	0.942 [0.932–0.951] 0.809	GLRLM_LRHGE, GLCM_Homogeneity, NGTDM_Coarseness, GLCM_Correlation, GLCM_Contrast
Dataset Ng = 128	0.860 0.830	0.985 0.795	0.949 [0.940–0.958] 0.843	GLRLM_LRHGE, NGTDM_Strength, GLSZM_HGZE, NGTDM_Coarseness, GLCM_Correlation
Dataset Ng = 256	0.853 0.785	0.990 0.589	0.945 [0.935–0.954] 0.841	GLRLM_LRHGE, NGTDM_Coarseness, GLCM_Correlation, GLRLM_SRE, NGTDM_Complexity

Table 3. *Radiomic model performance for the different grey levels (Ng). Accuracy, precision, and AUC are reported. The last column on the right describes the five features selected in each model.*

	GLRLM_LRHGE	NGTDM_Strength	GLSZM_HGZE	NGTDM_Coarseness	GLCM_Correlation
GLRLM_LRHGE	1.00				
NGTDM_Strength	0.54	1.00			
GLSZM_HGZE	0.43	0.81	1.00		
NGTDM_Coarseness	0.59	0.86	0.59	1.00	
GLCM_Correlation	0.44	0.44	0.48	0.37	1.00

Table 4. *Radiomic feature Pearson correlation coefficient used in the 128 grey-level model.*

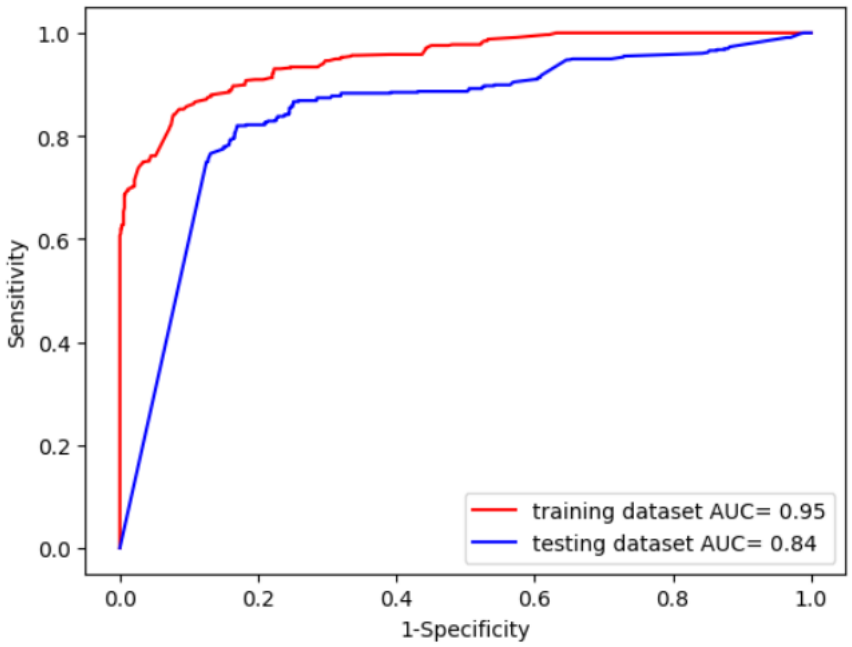

Figure 6. *ROC curves obtained in training and testing sets with relative AUCs for model using "Dataset Ng = 128".*

3.2 Part 2

The study cohort consisted of eight patients with biopsy-proven VRL (four males and four females; mean age 74 years), with a total of 22 visits and related image acquisitions and 43 eyes analysed (22 right, 21 left). Four patients did not have baseline OCT images because the instrument had not been available at the time of their diagnosis. Only one patient did not undergo the follow-up aqueous humour sampling in either eye due to death (for other reasons) before scheduling. Overall, 22 eyes were clinically classified as active disease, while 21 were considered inactive. We collected 15 samples of aqueous humour for molecular analyses. An IL-10:IL-6 ratio >1 was observed in seven eyes out of 15, whereas MYD88 mutations were detected in eight cases out of 13 analysable samples. IgH rearrangements were positive in all the analysable samples (eight cases), with seven missing determinations as the test was not performed due to the scarce quantity of aqueous humour, as in two cases for the MYD88. These descriptive characteristics are summarized in Table 5.

From the L2PO analysis, we obtained an AUC metric of 0.74 with a 95% CI range of 0.68–0.81, indicating that the metric remained stable for most of our patient clusters (Figure 6). The model with the best score showed an AUC of the test set of 0.78 (95% CI: 0.73–0.85); the model we selected is named "L2PO: test 3+7" and the five most important features chosen in this model were: GLRLM_LRLGE (IBSI: IVPO), HISTO_Skewness (IBSI: 88K1), GLCM_Correlation (IBSI: NI2N), HISTO_Variance (IBSI: CH89), GLRLM_LRHGE (IBSI: 3KUM). For complete nomenclature of the features, see https://ig-osiris.cancer.fr/ig/osiris/CodeSystem-IBSICS.html. We report the XGBoost parameters, feature selection result, model performances, and model explainability in Table 6 and Figures 7-9.

Overall, while some variables showed strong odds ratios, graphical inspection revealed limited discriminative power, with several associations driven by a few extreme observations.

GLRLM_LRLGE was the feature most consistently associated with disease activity. It showed association with clinical outcome across all statistical summaries (Table 7): mean (OR=2.51; p=0.015), median (OR=2.74; p=0.018), standard deviation (OR=11.27; p=0.035), 10th percentile (OR=3.26; p=0.028), and 90th percentile (OR=1.94; p=0.010).

When IL-10:IL-6 ratio >1 was used as the outcome, the associations weakened (all p-values >0.05), though mean and median values showed the same direction of effect (Table 8).

In Figures 10 and 11, the active VRL group shows a mild rightward shift and greater dispersion, yet substantial overlap with inactive eyes persists. The apparent significance thus reflects small-sample variability rather than a strong separation, suggesting limited clinical discriminative value despite robust ORs.

HISTO_variance was associated with IL-10:IL-6 ratio >1 (Table 8): mean (OR=10.27; p=0.029) and median (OR=9.34; p=0.047), though borderline results for 90th percentile (p = 0.058). For the clinical outcome, no significant relationship was found with HISTO_variance (Table 7). Plots in Figure 10 show broad variability with one evident outlier in the high-ratio group that strongly influences the regression, cautioning against excessive over-interpretation. In Figure 11, distributions are wide and largely overlapping, with only a modest rightward skew in the active disease group. Overall, HISTO_variance may have captured global heterogeneity in pixel intensity, but the apparent significance was driven by few extreme values and lacked clear separation between groups.

GLCM_correlation showed no appreciable association with clinical outcome (Table 7), but was weakly associated with IL-10:IL-6 ratio > 1 for mean (p=0.099) and median (p=0.062) values (Table 8). Graphical inspection suggests slightly higher values in eyes with elevated cytokine ratios, yet both density plots show extensive overlap, with no clear bimodality or thresholding effect. Thus, while GLCM_correlation may reflect subtle texture regularity differences, its predictive contribution appears negligible in this small cohort.

Across all outcomes, HISTO_skewness showed no appreciable association with either clinical activity or cytokine ratio (Tables 7 and 8). Figure 11 reveals flat or inconsistent relationships within IL-10:IL-6 ratio, and the density plots in Figure 12 overlap almost entirely. This indicates that histogram asymmetry does not provide a reliable signal of VRL activity in this dataset.

GLRLM_LRHGE showed a weak positive trend in the clinical model (OR range 1.13–1.83; all p-values >0.3. Table 7). No appreciable association was seen for IL-10:IL-6 ratio >1 (Table 8).

Visually, feature distributions of the groups are nearly superimposed, confirming the absence of discriminative capacity.

Overall, GLRLM_LRLGE emerged as the most reproducible descriptor, showing consistent though moderate associations with disease activity. HISTO_variance and GLCM_correlation exhibited partial or cytokine-specific trends, whereas HISTO_skewness and GLRLM_LRHGE provided no useful signal.

Radiomic feature analysis shows that a high GLRLM_LRLGE value indicates extensive areas with relatively low intensity. Positive HISTO_skewness means a long right tail in the grey-level histogram, while negative skewness signifies the opposite. High GLCM_correlation values point to a strong linear relationship between grey levels, related to smoother textures, whereas low values suggest greater randomness. Elevated HISTO_variance indicates a broader range of intensity distribution. Lastly, high GLRLM_LRHGE values identify long runs of high-intensity pixels, highlighting large bright regions. Overall, these parameters serve as heterogeneity indicators, each capturing different aspects of non-uniformity in grey-level intensity and texture within the image.

Model's explainability supported these interpretations. In the SHAP summary plot, GLRLM_LRLGE shows the largest and most consistently positive impact on the model output, indicating that extended runs of low grey levels drive predictions toward the positive class (active VRL). Higher GLCM_correlation values also tend to have positive SHAP contributions, consistent with smoother, more linearly related grey levels influencing the decision. HISTO_skewness exhibits a similar pattern. GLRLM_LRHGE generally shows positive contributions at higher values, in line with long homogeneous runs of high intensity, favouring the active VRL group due to high cellular density in the image. By contrast, higher HISTO_variance is associated with the inactive group or mixed SHAP values, suggesting that the model interpreted a broad intensity spread as evidence against the active disease class. Overall, these patterns confirm that the most influential predictors are texture-based measures capturing different facets of grey-level non-uniformity, reinforcing their shared role as heterogeneity descriptors.

Patient ID	Sex	Year of birth	ANTERION Imaging collection date	Eye laterality Imaging (R=right; L=left)		Clinical outcome (0=inactivity; 1= active disease)		Paracentesis eye laterality (R=right; L=left)		IL-10:IL-6 ratio > 1 outcome (0=inactivity; 1= active disease)		IL-10:IL-6 ratio	MYD88	IgH
001	M	1957	10/2023	R	L	0	1	-	L	-	1	1.04	Pos	-
			12/2023	R	L	0	0	-	-	-	-	-	-	-
			02/2024	R	L	0	1	-	L	-	1	5.23	Pos	Pos
002	F	1951	01/2022 (TOD)	R	L	1	1	R	-	1	-	111.93	Neg	Pos
			04/2023	R	L	1	0	-	-	-	-	-	-	-
			07/2023	R	L	1	0	-	L	-	0	0.01	Neg	-
			11/2023	R	L	0	0	R	-	0	-	0.00	Neg	-
003	F	1940	12/2022	R	-	0	-	R	-	0	-	0.00	-	-
			01/2024	R	L	0	0	-	-	-	-	-	-	-
004	F	1964	04/2022 (TOD)	R	L	1	1	-	L	-	1	12.16	Pos	-
			11/2022	R	L	0	0	-	-	-	-	-	-	-
			11/2023	R	L	0	0	R	-	0	-	0.02	Neg	Pos
005	M	1949	11/2022 (TOD)	R	L	1	1	R	-	0	-	0.52	Pos	Pos
			02/2024	R	L	1	1	-	L	-	0	0.04	-	Pos
006	M	1946	11/2022	R	L	0	0	-	-	-	-	-	-	-
			06/2023	R	L	1	1	R	-	1	-	6.05	Pos	-
			10/2023	R	L	1	1	-	-	-	-	-	-	-
			11/2023	R	L	1	1	R	-	1	-	4.98	Pos	Pos
			02/2024	R	L	1	1	R	-	1	-	27.51	Pos	Pos
007	F	1946	08/2023 (TOD)	R	L	1	0	-	L	-	0	0.02	Pos	-
			11/2023	R	L	1	0	-	-	-	-	-	-	-
008	M	1961	09/2023	R	L	0	0	R	-	0	-	0.02	Neg	Pos

Table 5. *Descriptive characteristics of the study cohort. Overall, 8 patients were included, with 22 visits and 43 eyes evaluated (22 right, 21 left). Clinical outcome: 21 inactive diseases, 22 active diseases. IL-10:IL-6 >1 outcome: 7 cases out of 15. MYD88 positive outcome: 8 eyes out of 13. IgH rearrangements positive outcome: 8 cases out of 8. The results of MYD88 and IgH rearrangements were not divided into right and left eyes because their data derive from the analysis of the same samples on which the IL-10:IL-6 ratio was quantified and it was not possible to carry out such further molecular analyses for all the samples.*

Parameter	Value
'colsample_bytree'	0.084829
'gamma'	1.543222
'learning_rate'	0.099942
'min_child_weight'	8
'max_depth'	18
'n_estimators'	158
'subsample'	0.673114
'eval_metric'	'auc'
'seed'	0
'early_stopping_rounds'	10

Table 6. *Optimal XGBoost model parameter calculated.*

	Clinical outcome					
	inactive disease n=21 mean (SD)	active disease n=22 mean (SD)	OR	p-value	95% CI	
mean						
glcm_correlation	-0.21 (1.20)	-0.43 (0.73)	0.789	0.467	0.079	1.747
histo_skewness	0.33 (0.13)	0.06 (0.59)	0.709	0.389	0.315	1.60
histo_variance	-0.08 (0.95)	-0.28 (0.54)	0.690	0.436	0.261	1.826
glrlm_lrhge	-0.00 (1.08)	0.26 (1.14)	1.255	0.409	0.717	2.196
glrlm_lrlge	-0.17 (0.45)	0.58 (1.28)	2.510	0.015	1.221	5.159
median						
glcm_correlation	-0.17 (1.23)	-0.42 (0.80)	0.787	0.436	0.419	1.474
histo_skewness	0.28 (0.12)	-0.03 (0.59)	0.668	0.315	0.296	1.509
histo_variance	-0.08 (0.96)	-0.32 (0.50)	0.646	0.351	0.249	1.676
glrlm_lrhge	-0.06 (1.05)	0.25 (1.19)	1.300	0.317	0.763	2.217
glrlm_lrlge	-0.23 (0.41)	0.46 (1.21)	2.735	0.018	1.207	6.196
standard deviation						
glcm_correlation	0.33 (0.17)	0.42 (0.19)	17.791	0.159	0.294	1,077.770
histo_skewness	0.44 (0.22)	0.49 (0.19)	3.339	0.442	0.136	81.893
histo_variance	0.26 (0.32)	0.25 (0.27)	0.928	0.957	0.054	15.808
glrlm_lrhge	0.30 (0.35)	0.37 (0.36)	1.828	0.570	0.208	16.073
glrlm_lrlge	0.25 (0.17)	0.55 (0.53)	11.268	0.035	1.214	104.592
10th percentile						
glcm_correlation	-0.60 (1.16)	-0.94 (0.69)	0.676	0.226	0.357	1.299
histo_skewness	-0.21 (1.03)	-0.47 (0.47)	0.643	0.356	0.243	1.701
histo_variance	-0.40 (0.62)	-0.60 (0.22)	0.324	0.181	0.059	1.765
glrlm_lrhge	-0.31 (0.80)	-0.21 (0.64)	1.223	0.648	0.489	3.083
glrlm_lrlge	-0.40 (0.36)	0.04 (0.82)	3.261	0.028	1.147	9.273
90th percentile						
glcm_correlation	0.15 (1.23)	0.12 (0.73)	0.973	0.937	0.477	1.984
histo_skewness	0.90 (1.35)	0.76 (0.83)	0.886	0.699	0.467	1.698
histo_variance	0.27 (1.36)	0.07 (0.93)	0.858	0.646	0.434	1.698
glrlm_lrhge	0.45 (1.52)	0.72 (1.53)	1.130	0.569	0.728	1.754
glrlm_lrlge	0.13 (0.55)	1.29 (1.89)	1.944	0.010	1.194	3.165

Table 7*. Univariate logistic regression models for clinical outcome (inactive vs. active disease). Odds ratios (OR) with 95% confidence intervals (CI) and p-values are reported for each radiomic feature across different statistical measures (mean, median, standard deviation, 10th percentile and 90th percentile).*

	IL10:IL6 ratio >1					
	inactive disease n=8 mean (SD)	active disease n=7 mean (SD)	OR	p-value	95% CI	
mean						
glcm_correlation	-0.72 (0.67)	-0.17 (0.66)	4.267	0.099	0.734	24.799
histo_skewness	0.40 (0.54)	0.15 (0.82)	0.542	0.428	0.108	2.712
histo_variance	-0.54 (0.12)	-0.19 (0.66)	10.271	0.029	1.319	79.973
glrlm_lrhge	0.06 (1.24)	0.10 (1.10)	1.038	0.939	0.365	2.958
glrlm_lrlge	0.18 (1.05)	0.40 (1.11)	1.247	0.693	0.386	4.026
median						
glcm_correlation	-0.71 (0.69)	-0.10 (0.62)	5.134	0.062	0.910	28.967
histo_skewness	0.32 (0.55)	0.07 (0.80)	0.536	0.422	0.107	2.698
histo_variance	-0.55 (0.12)	-0.25 (0.60)	9.336	0.047	1.038	84.008
glrlm_lrhge	0.02 (1.21)	0.07 (1.10)	1.037	0.943	0.358	3.004
glrlm_lrlge	0.09 (1.01)	0.31 (1.02)	1.275	0.685	0.362	4.492
standard deviation						
glcm_correlation	0.34 (0.21)	0.40 (0.18)	4.531	0.605	0.009	2,085.853
histo_skewness	0.47 (0.20)	0.58 (0.25)	12.666	0.316	0.067	2,374.786
histo_variance	0.14 (0.05)	0.29 (0.29)	194.925	0.075	0.544	69,825.720
glrlm_lrhge	0.27 (0.32)	0.32 (0.33)	1.816	0.744	0.039	83.915
glrlm_lrlge	0.42 (0.43)	0.41 (0.31)	0.859	0.918	0.038	19.267
10th percentile						
glcm_correlation	-1.10 (0.57)	-0.71 (0.69)	3.028	0.342	0.270	33.905
histo_skewness	-0.13 (0.39)	-0.53 (0.64)	0.176	0.109	0.020	1.549
histo_variance	-0.69 (0.07)	-0.53 (0.31)	63.059	0.085	0.523	7,604.937
glrlm_lrhge	-0.24 (0.92)	-0.27 (0.69)	0.941	0.929	0.221	4.012
glrlm_lrlge	-0.22 (0.63)	-0.04 (0.82)	1.458	0.632	0.279	7.621
90th percentile						
glcm_correlation	-0.33 (0.86)	0.32 (0.67)	3.541	0.066	0.908	13.800
histo_skewness	1.03 (0.76)	1.02 (1.15)	0.984	0.980	0.264	3.670
histo_variance	-0.38 (0.16)	0.23 (1.06)	6.429	0.058	0.933	44.304
glrlm_lrhge	0.40 (1.60)	0.54 (1.49)	1.069	0.858	0.483	2.370
glrlm_lrlge	0.64 (1.50)	1.04 (1.69)	1.119	0.632	0.541	2.660

Table 8. *Univariate logistic regression models for IL10:IL6 ratio outcome (inactive vs. active disease). Odds ratios (OR) with 95% confidence intervals (CI) and p-values are reported for each radiomic feature across different statistical measures (mean, median, standard deviation, 10th percentile and 90th percentile).*

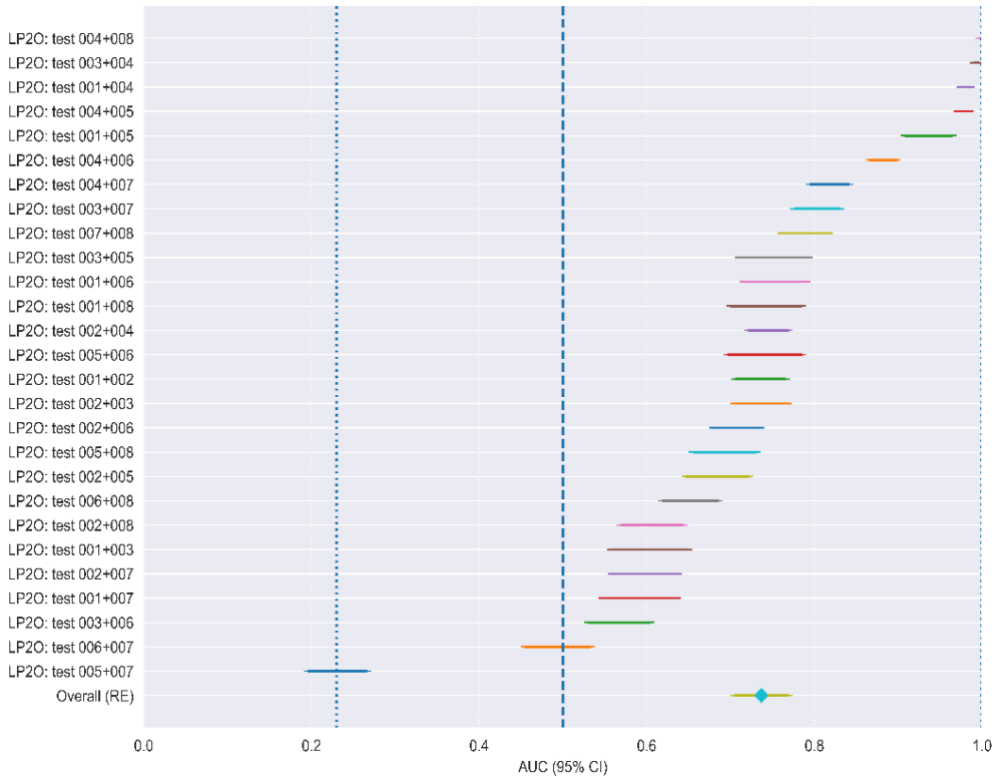

***Figure 7**. Performance across leave-two-patients-out (L2PO) cross-validation. Each horizontal bar reports the AUC with 95% CI for the test fold defined by the two held-out patients (listed at left); the model was trained on all remaining patients (n–2) for each fold to avoid subject leakage. The diamond shows the overall AUC pooled across folds using a random-effects model. Vertical dashed lines mark AUC = 0.25, 0.5, and 1.0.*

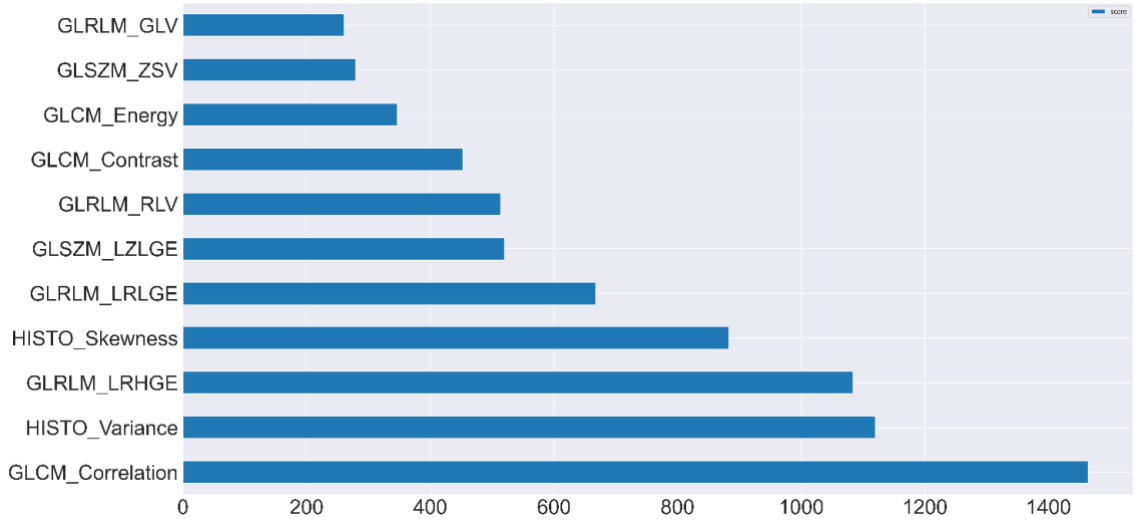

***Figure 8**. Feature importance.*

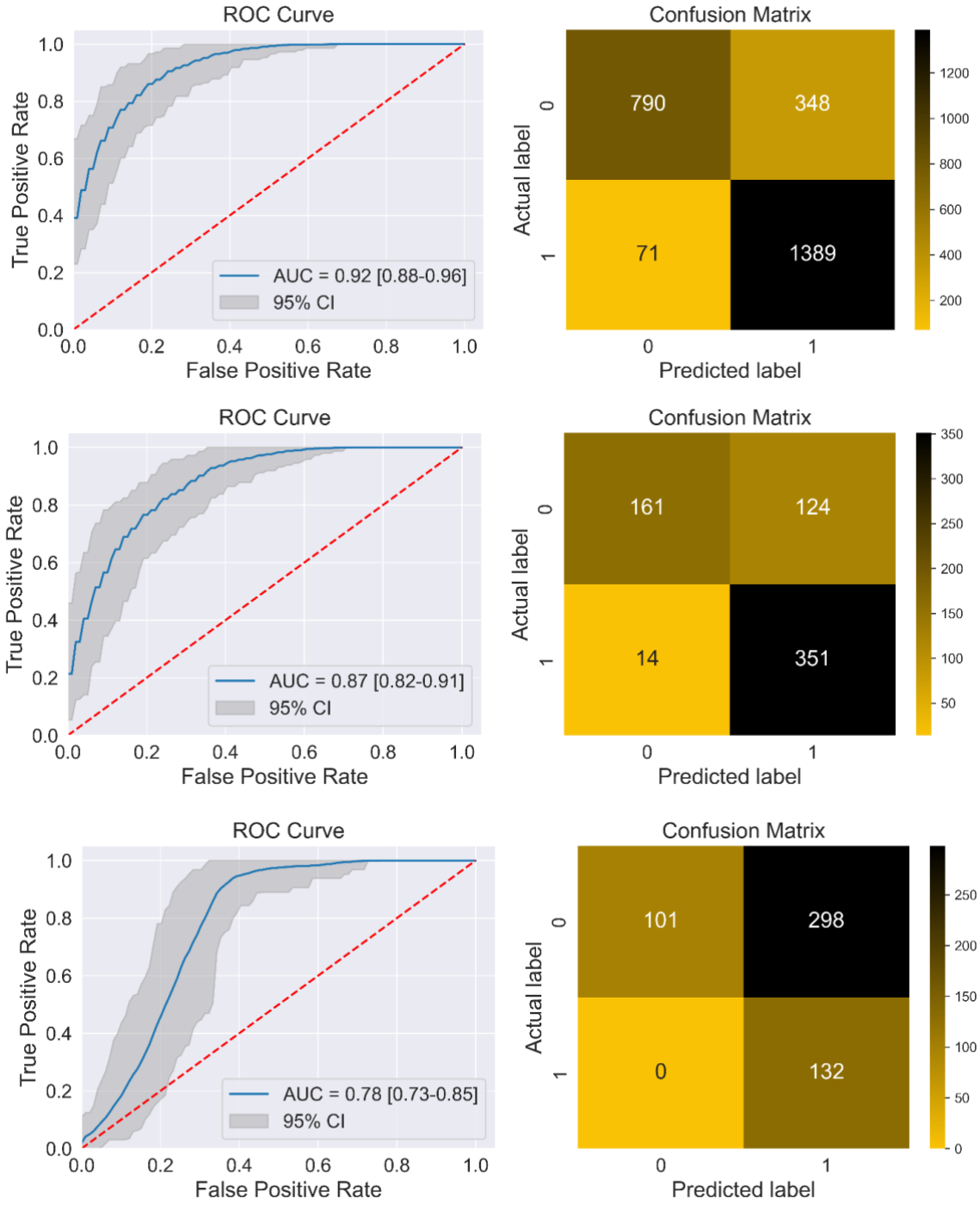

Figure 9. *Model performance on the Training (top), Validation (middle), and Testing (bottom) datasets.*

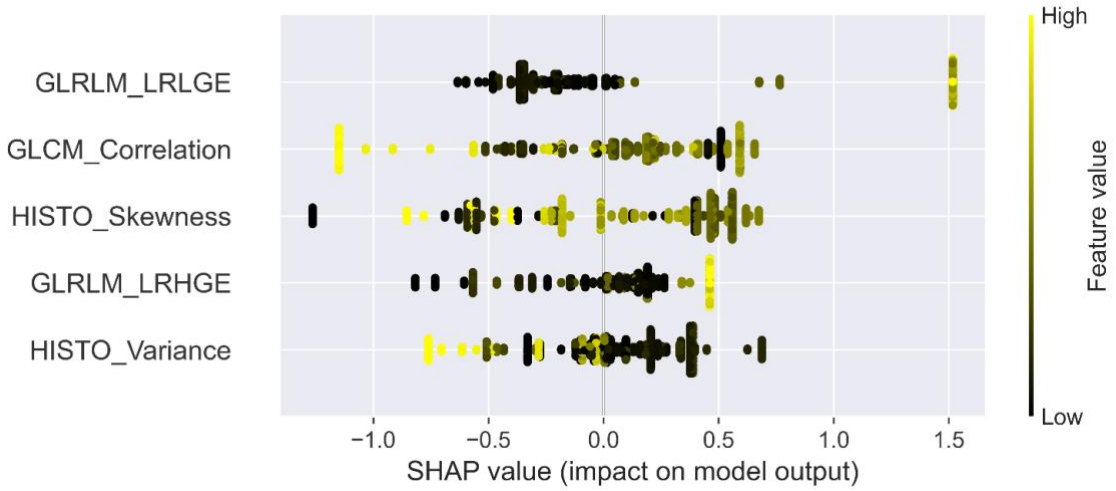

Figure 10. *SHapley Additive exPlanations (SHAP) beeswarm summary plot.*

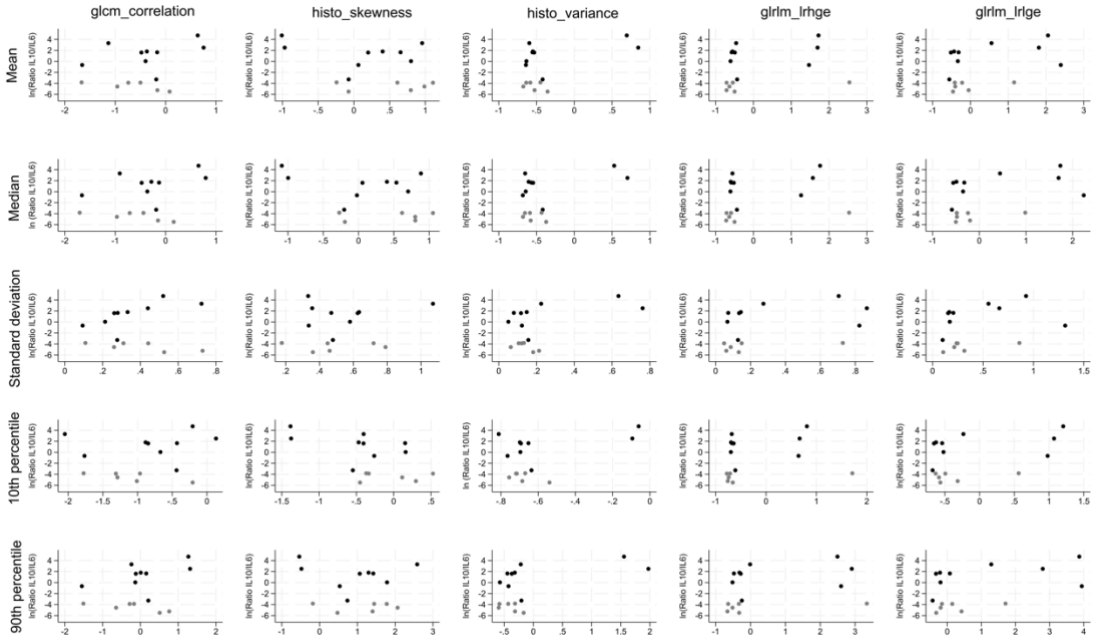

Figure 11. *Relationships between mean, median, standard deviation, 10th percentile and 90th percentile of the selected radiomic features and the logarithm of IL-10:IL-6 ratios. Black points indicate active disease, and grey points indicate inactive disease.*

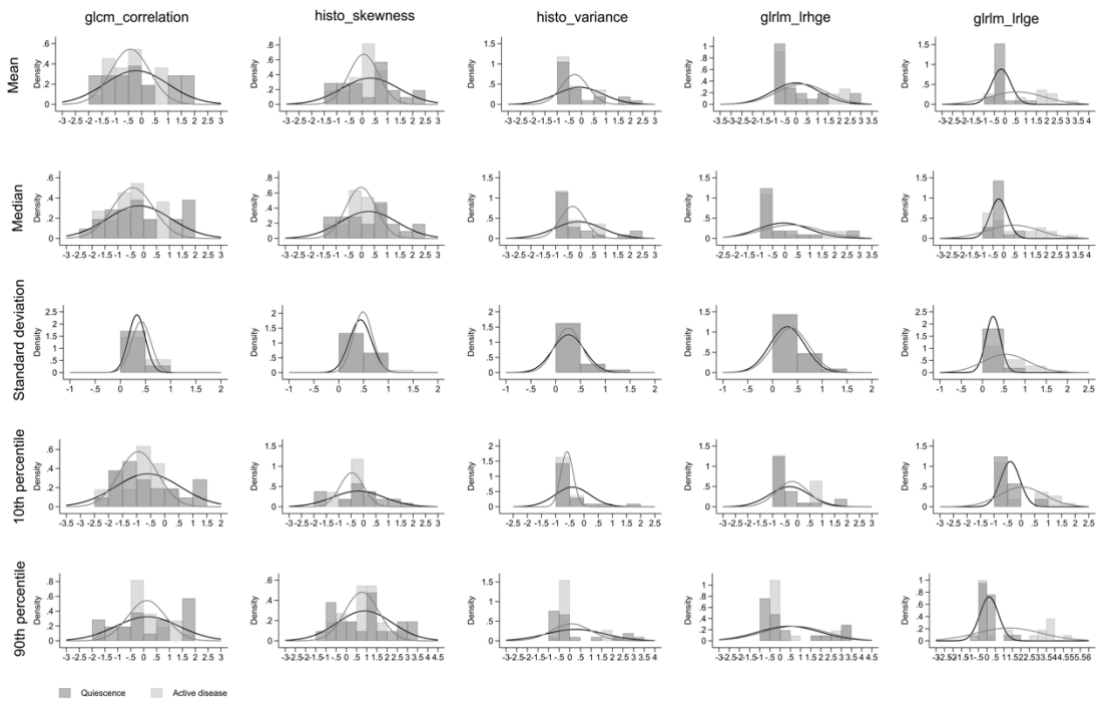

Figure 12. *Density plots of the mean, median, standard deviation, 10th percentile and 90th percentile of the selected radiomic features. Darker grey refers to inactive disease.*

4. DISCUSSION

4.1 Part 1

The incidence of VRL has increased over the last decades thanks to improvements in diagnostics and advances in health care, resulting in longer life expectancies. It must be emphasised that patients later found to be affected by VRL are being referred more frequently to a uveitis specialist because these tumours may mimic inflammatory eye disease. For this reason, recognising VRL, especially, in differential diagnosis with uveitis is a great challenge; the high rate of diagnostic delay worsens not only the visual prognosis, it also, and more importantly, shortens the patient's life. It is important to objectively discriminate between vitreous infiltration in VRL and vitreous inflammation in uveitis. Indeed, the former has characteristics that are so beyond clinical uveitis grading that it can be defined as "muddy", corresponding to aurora borealis and string of pearls in ultrawide-field imaging. Vitreous morphological characteristics are traceable to two

different etiopathogenic pathways: inflammation in the case of uveitis and cancer in the case of VRL.[10]

Multimodal imaging could aid in detecting "muddy" vitreous. The only imaging valuable for diagnosing VRL is currently that of the posterior segment.[51] Our study evaluated the possible usefulness of the AS-OCT in diagnosing this rare but dangerous tumour. To obtain this result, we based our predictive model on biopsy-proven lymphomatous cases to distinguish between vitreous involvement in VRL and vitritis. To verify the accuracy of AS-OCT, data from 28 patients (11 with biopsy-proven VRL and 17 with differential diagnosis uveitis) were used to train and test our model's performance.

Our results show that age did not influence the model outcome. On the one hand, it is true that the vitreous undergoes morphological changes with age, leading to an increase in opacities perceived as floaters, which sometimes functionally disturb vision (the so-called "vision degrading myodesopsia").[67] On the other hand, it has recently been highlighted that the structural and morphological alterations of the anterior vitreous can be analysed with OCT, which is able to distinguish between the vitreous cisterns and lacunae, which are hyporeflective, and the hyper-reflective macromolecular aggregates of collagen that form the bundles of linear fibrils typical of the aging vitreous.[68,69]

This is the first study that evaluates radiomics in uveitis. However, in ophthalmology, radiomic models have been preliminarily studied in diabetic retinopathy, retinal venous occlusions, and relative response to anti-vascular endothelial growth factors (VEGF).[70,71] The basis of radiomics consists of extracting well-defined, hand-crafted features from the image pixels in order to grasp what is not explainable using the clinician's eye.[72,73] Indeed, looking at the OCT scans of the anterior vitreous, clinicians would not be able to distinguish between vitreous involvement due to VRL or vitritis. On the contrary, radiomics performs a mathematical analysis on each single OCT capture, so it is able to catch differences in the pattern of all analysed images. It allowed us to reach the correct diagnosis in 87% of eyes and in 82% of patients. Our study shows that radiomic processing of the AS-OCT images could be an important supportive test helping the clinician in the diagnostic pathway of VRL.

It is important to note that we did not use the acquisition method as a feature to train the models because it would have been a bias, given the retrospective nature of this study. Due to the rarity of VRL, it is very difficult to collect a sizable cohort of these patients.

Based on the results listed in Table 4, we found that several features were collinear, which could cause a problem with the proposed radiomic model. However, the xgboost algorithm was not affected by collinearity issues because it consisted of a decision tree ensemble classifier.

Our research shows that using a higher number of grey levels can highlight finer variations in the image as well as the complexity of their arrangement in the vitreous chamber. On the contrary, too many grey levels may introduce a bias in the model prediction caused by image noise. Decreasing the number of levels is a sort of complexity reduction, meaning that their ability to detect different details in the vitreal cavity diminishes. A trade-off must be considered; our analysis found it in 128 grey levels. The selected features to build radiomic models have in common their ability to describe how the higher number of pixels (normal vitreous tends to be represented with zero values) are arranged, and their relative displacement is better described in models with higher grey levels.

There has recently been an increasing number of studies employing deep learning in differential diagnosis. However, we decided to use a machine learning method because we did not have a sufficient number of patients/eyes available due to VRL being a rare pathology. The optimal starting point should be to adopt machine learning methods to assess the feasibility of using AI techniques for this unexplored kind of imaging. A future deep learning-based study is possible, provided there are more data.[74]

In summary, the strength of this work is the relative simplicity of application of the described method based on a machine learning technique that allows calculating a probability of discrimination of VRL in a short time. Moreover, this study has some limitations. First, the retrospective nature of the analysis limited the consistency of the data. Second, the small sample size decreased the power of our statistical analysis. Third, this was a single-centre study. Because of these limitations, we could not perform a harmonisation of our data because it was not possible to apply the methods described in the literature.[75-78]

In conclusion, this preliminary retrospective study highlights how the AS-OCT can support the clinician in suspected VRL. Clearly, it should be emphasised that it is still necessary to collect a vitreous and/or aqueous sample to confirm a diagnosis, but AS-OCT is a quick and easy-to-use additional tool for deciding whether a diagnostic

vitrectomy is required. This makes it possible to achieve the goal of reducing diagnostic delay, which would improve not only the patient's visual prognosis but above all the quoad vitam prognosis. Further multicentre studies with a larger population sample are needed to confirm our results.

4.2 Part 2

In this exploratory study, after extracting radiomic features information from AS-OCT images, we built predictive models to distinguish between active and inactive VRL. We used an L2PO technique to address eventual biases and to reduce overfitting. Our models showed a median AUC of 0.74 (95% CI: 0.68–0.81), indicating that the metric was stable within the patient clusters used.

We identified several radiomic features that demonstrated strong associations with active VRL. Among these, GLRLM_LRLGE emerged as the most consistent descriptor, showing strong correlations across multiple distributional summaries with active disease status. HISTO_variance and GLCM_correlation also displayed suggestive associations with the IL-10:IL-6 ratio, supporting the hypothesis that local textural heterogeneity within the analysed anterior vitreous could reflect cellular activity. However, we would like to highlight that these features quantify the variability and spatial organization of pixel intensities rather than any directly measurable biological property. Consequently, their interpretation should remain strictly image-based: they represent intrinsic statistical patterns of the OCT signal, not morphological or cellular correlates. Model explainability (SHAP analysis) confirmed that the most influential features were those describing local intensity dispersion and texture uniformity, reinforcing that radiomics primarily captures heterogeneity-related aspects of image structure.

Overall, no single radiomic parameter achieved a discriminative performance sufficient for clinical application. The partial overlap of feature distributions between active and inactive eyes indicates that radiomics alone, in its current form, cannot reliably determine VRL disease activity.

Importantly, across all variables, visual plots reveal that most differences were small and often driven by isolated data points. Thus, although some features reached statistical significance, their biological or diagnostic meaning remains uncertain, and they should be interpreted as indicators of imaging heterogeneity rather than true disease markers.

To date, no other study has specifically explored radiomic analysis of AS-OCT images in predicting active or inactive VRL. Previous investigations in ophthalmology have focused on texture-based image analysis for anterior and posterior segment inflammation, showing correlations between OCT-derived parameters and clinical grading of anterior chamber inflammation or vitreous haze. In fact, OCT-based approaches such as anterior chamber cells and flare quantification and posterior vitreous density mapping offer indirect but non-invasive insight, although none have yet achieved standardization or widespread clinical adoption in uveitis.[48] Instead, in oncology, radiomics has been extensively applied for tumour classification, response prediction, and minimal residual disease detection, supporting the conceptual transferability of this approach to ocular oncology.[79]

Alternative strategies for non-invasive VRL monitoring remain limited. Serial IL-10:IL-6 quantification, MYD88 L265P detection, and IgH clonality testing from aqueous humour have been proposed as surrogate biomarkers, but all require aqueous tap and suffer from inconsistent reproducibility. In this context, our pilot study represents the first step toward quantitative, image-based monitoring of VRL.[52]

The main limitation of our study is its small sample size, which is inherent to VRL studies given the rarity of this disease; the small sample size therefore restricted both the study's statistical power and the generalizability of our findings.

A further challenge was that there is no universally accepted gold standard for intraocular VRL activity assessment. We therefore adopted a pragmatic composite reference that integrated clinical examination, laboratory results (IL-10:IL-6 ratio, MYD88, IgH), physician decision to modify therapy and longitudinal follow-up. This strategy has a strong clinical rationale but may have introduced heterogeneity as clinical decisions and biomarker fluctuations can be context-dependent.

Another limitation is related to the radiomics pipeline itself: each AS-OCT image represents only a portion of the anterior vitreous, and variations in scan position and image quality can influence feature extraction. Despite implementing quality thresholds and cross-validation, residual technical variability cannot be excluded.

Lastly, MYD88 L265P mutation and IgH clonality assays in our cohort were almost uniformly positive whenever active disease was present. While it is tempting to interpret this as near-perfect sensitivity, we consider it more likely an artefact of limited sample

size and homogeneity. In fact, it is known that VRL exists even in the absence of MYD88 mutation and IgH rearrangements.[2] Finally, since few aqueous taps were performed because of its invasiveness, the availability of complementary biological validation was limited.

Despite its limitations, this study also has significant strengths. First of all, the idea of applying an artificial intelligence method in a still highly under-explored pathology such as VRL is original. The fully quantitative non-invasive imaging approach of this study is innovative because nowadays the quantitative determination of VRL activity is still based on the aqueous tap. Furthermore, our study presents a reproducible processing pipeline, as illustrated in the radiomic framework of the methods. Last but not least, seeking an integration with biomolecular data is an important strength since these data currently constitute a fundamental diagnostic tool for evaluating VRL activity.

Our results indicate that AS-OCT images carry latent information related to VRL activity that can be quantitatively extracted through radiomic analysis. Although none of the individual features achieved robust discrimination, when taken together, they showed promising predictivity of clinical outcomes.

Future research should focus on expanding the dataset to allow the development of multi-feature predictive models, possibly by integrating radiomic, molecular, and clinical parameters. In fact, a combined approach that integrates radiomic features and aqueous humour biomarkers could enhance the robustness of disease-monitoring models. If validated, this model could help to identify patient subgroups where invasive sampling can be avoided, for instance, in eyes whose radiomic profiles are characterized by high positive or negative predictive value for active or inactive VRL, respectively. Any treatment in these cases could be determined even in the absence of an aqueous tap, which would be reserved only for those patients with residual uncertainty.

In conclusion, the findings of this pilot start-up study suggest that radiomics-based texture analysis may hold potential for assessing VRL active disease through AS-OCT and reinforce the hypothesis that radiomics could become a non-invasive adjunct tool for disease monitoring, thereby supporting precision-based management in VRL. Although partial overlap between radiomic patterns in active and inactive eyes limits definitive discrimination at this stage, these preliminary findings indicate that radiomics could

represent a meaningful objective for future investigations aiming to refine non-invasive diagnostic strategies.

Key points:

- VRL is often mistaken for uveitis, significantly delaying the diagnosis and markedly worsening the patient's prognosis.
- Cytology remains the diagnostic gold standard for VRL, although its sensitivity is suboptimal.
- Ancillary tests on ocular fluids allow for an improved ability to diagnose vitreoretinal lymphoma. Currently, the most widely used are the IL-10/IL-6 ratio, the presence of mutations in the MYD88 gene, and the presence of rearrangements in the immunoglobulin heavy chains.
- Firstly, we explored the ability of AS-OCT in distinguishing lymphocytic infiltration from inflammatory infiltration within the anterior vitreous by using a radiomic classification model.
- We built a classification model, through which 87% of eyes were correctly diagnosed as VRL or uveitis. AUCs in the 128 grey-level model were 0.95 [CI 0.94, 0.96] and 0.84 for training and testing datasets, respectively.
- Secondly, we investigated the ability of a radiomics-based classification model to identify AS-OCT image features compatible with active VRL (recurrence). The secondary aim was to investigate the possible association between the results of this non-invasive method and the aqueous tap molecular biomarkers currently used to determine VRL disease activity.
- We obtained an AUC metric of 0.74 [CI 0.68–0.81]. GLRLM_LRLGE was the feature most consistently associated with disease activity. When IL-10:IL-6 >1 was used as the outcome, the association weakened (all p-values >0.05), though mean and median values showed the same direction of effect.
- These are the first attempts to evaluate the capabilities of AS-OCT in the differential diagnosis between VRL and uveitis, and in identifying the recurrence of VRL. Studies with a larger patient cohort are necessary to confirm our results.

5. REFERENCES

1. Wang SY, Zhou SW, Gao J, Wang L. Primary vitreoretinal lymphoma: diagnosis, treatment, and prognosis - a review of current knowledge and future directions. Vol. 7, Blood Science. Lippincott Williams and Wilkins; 2025.
2. Melli B, Gentile P, Nicoli D, Farnetti E, Croci S, Gozzi F, Bolletta E, De Simone L, Sanguedolce F, Palicelli A, Zizzo M, Ricci S, Ilariucci F, Rossi C, Cavazza A, Ascani S, Cimino L, Zanelli M. Primary Vitreoretinal Lymphoma: Current Diagnostic Laboratory Tests and New Emerging Molecular Tools. Curr Oncol. 2022 Sep 24;29(10):6908-6921.
3. Hong JT, Chae JB, Lee JY, Kim JG, Yoon YH. Ocular involvement in patients with primary CNS lymphoma. J Neurooncol. 2011 Mar;102(1):139–45.
4. Chan CC, Rubenstein JL, Coupland SE, Davis JL, Harbour JW, Johnston PB, et al. Primary Vitreoretinal Lymphoma: A Report from an International Primary Central Nervous System Lymphoma Collaborative Group Symposium. Oncologist. 2011 Nov 1;16(11):1589–99.
5. Batchelor TT. Primary central nervous system lymphoma: A curable disease. Hematol Oncol. 2019 Jun 1;37(S1):15–8.
6. Cho BJ, Kim DY, Park UC, Lee JY, Yoon YH, Yu HG. Clinical Features and Treatment Outcomes of Vitreoretinal Lymphoma according to Its Association with CNS Lymphoma. Ocul Immunol Inflamm. 2018 Apr 3;26(3):365–71.
7. Sobolewska B, Chee SP, Zaguia F, Goldstein DA, Smith JR, Fend F, Mochizuki M, Zierhut M. Vitreoretinal Lymphoma. Cancers (Basel). 2021 Aug 4;13(16):3921.
8. Margolis L, Fraser R, Lichter A, Char DH. The role of radiation therapy in the management of ocular reticulum cell sarcoma. Cancer. 1980 Feb 15;45(4):688–92.
9. BUETTNER H, BOLLING JP. Intravitreal Large-Cell Lymphoma. Mayo Clin Proc. 1993;68(10):1011–5.
10. Carbonell D, Mahajan S, Chee SP, Sobolewska B, Agrawal R, Bülow T, Gupta V, Jones NP, Accorinti M, Agarwal M, Batchelor T, Biswas J, Cimino L, tenDam-van Loon NH, de-la-Torre A, Frenkel S, Pe'er J, Kramer M, Miserocchi E, Mochizuki M, Ness T, Rosenbaum JT, Sen HN, Simion M (VRL patient), Sitter H, Vasconcelos-Santos DV, Habot-Wilner Z, Coupland SE, Pulido JS, Smith J, Thorne JE, Zierhut M; Study Group for Vitreoretinal Lymphoma Diagnostics. Consensus Recommendations for the Diagnosis of Vitreoretinal Lymphoma. Ocul Immunol Inflamm. 2021 Apr 3;29(3):507-520.
11. Sagoo MS, Mehta H, Swampillai AJ, Cohen VML, Amin SZ, Plowman PN, et al. Primary intraocular lymphoma. Vol. 59, Survey of Ophthalmology. Elsevier USA; 2014. p. 503–16.
12. Lee J, Kim SW, Kim H, Lee CS, Kim M, Lee SC. DIFFERENTIAL DIAGNOSIS FOR VITREORETINAL LYMPHOMA WITH VITREORETINAL FINDINGS, IMMUNOGLOBULIN CLONALITY TESTS, AND INTERLEUKIN LEVELS. Retina. 2019 Jun;39(6):1165–76.
13. Levasseur SD, Wittenberg LA, White VA. Vitreoretinal lymphoma: a 20-year review of incidence, clinical and cytologic features, treatment, and outcomes. JAMA Ophthalmol. 2013 Jan;131(1):50–5.
14. Chan CChao, Gonzales JA. Primary intraocular lymphoma. World Scientific; 2007. 284 p.

15. Marchese A, Miserocchi E, Giuffrè C, Cicinelli MV, Querques G, Bandello F, et al. Aurora borealis and string of pearls in vitreoretinal lymphoma: Patterns of vitreous haze. British Journal of Ophthalmology. 2019 Nov 1;103(11):1656–9.
16. Araujo I, Coupland SE. Primary Vitreoretinal Lymphoma -- A Review. Asia Pac J Ophthalmol (Phila). 2017 May-Jun;6(3):283-289.
17. Coupland SE, Perez-Canto A, Hummel M, Stein H, Heimann H. Assessment of HOPE fixation in vitrectomy specimens in patients with chronic bilateral uveitis (masquerade syndrome). Graefe's Archive for Clinical and Experimental Ophthalmology. 2005 Sep;243(9):847–52.
18. Coupland SE. Analysis of intraocular biopsies. Dev Ophthalmol. 2012;49:96–116.
19. Ito T, Takeda A, Fujiwara K, Hasegawa E, Nakao S, Ohishi Y, Oda Y, Yoshikawa H, Sonoda KH. Risk factors for failure of vitrectomy cell block technique in cytological diagnosis of vitreoretinal lymphoma. Graefes Arch Clin Exp Ophthalmol. 2019 May;257(5):1029-1036.
20. Missotten T, Tielemans D, Bromberg JE, Van Hagen PM, Van Lochem EG, Van Dongen JJM, et al. Multicolor flowcytometric immunophenotyping is a valuable tool for detection of intraocular lymphoma. Ophthalmology. 2013 May;120(5):991–6.
21. Davis JL, Ruiz P, Shah M, Mandelcorn ED. Evaluation of the reactive T-cell infiltrate in uveitis and intraocular lymphoma with flow cytometry of vitreous fluid (an American Ophthalmological Society thesis) [Internet]. Vol. 110, Trans Am Ophthalmol Soc. 2012.
22. Hardy RR, Hayakawa K. B cell development pathways [Internet]. 2001. Available from: www.annualreviews.org
23. Katai N, Kuroiwa S, Fujimori K, Yoshimura N, Katai N, Kuroiwa) -S, et al. Diagnosis of intraocular lymphoma by polymerase chain reaction. Vol. 235, Arch Clin Exp Ophthatmol. 1997.
24. Coupland SE, Hummel M, Müller HH, Stein H. Molecular analysis of immunoglobulin genes in primary intraocular lymphoma. Invest Ophthalmol Vis Sci. 2005 Oct;46(10):3507–14.
25. Merle-Béral H, Davi F, Cassoux N, Baudet S, Colin C, Gourdet T, et al. Biological diagnosis of primary intraocular lymphoma. Br J Haematol. 2004 Feb;124(4):469–73.
26. Wang Y, Shen D, Wang VM, Sen HN, Chan CC. Molecular biomarkers for the diagnosis of primary vitreoretinal lymphoma. Int J Mol Sci. 2011 Sep;12(9):5684–97.
27. Bonzheim I, Giese S, Deuter C, Süsskind D, Zierhut M, Waizel M, et al. High frequency of MYD88 mutations in vitreoretinal B-cell lymphoma: A valuable tool to improve diagnostic yield of vitreous aspirates. Blood. 2015 Jul 2;126(1):76–9.
28. Chan CC, Whitcup SM, Solomon D, Nussenblatt RB. Interleukin-10 in the vitreous of patients with primary intraocular lymphoma. Am J Ophthalmol. 1995;120(5):671–3.
29. Kuo DE, Wei MM, Knickelbein JE, Armbrust KR, Yeung IYL, Lee AY, et al. Logistic Regression Classification of Primary Vitreoretinal Lymphoma versus Uveitis by Interleukin 6 and Interleukin 10 Levels. Ophthalmology. 2020 Jul 1;127(7):956–62.
30. Costopoulos M, Touitou V, Golmard JL, Darugar A, Fisson S, Bonnemye P, et al. ISOLD: A New Highly Sensitive Interleukin Score for Intraocular Lymphoma Diagnosis. Journal of The American Academy of Ophthalmology [Internet]. 2016;123(7):1626–8.
31. Cani AK, Hovelson DH, Demirci H, Johnson MW, Tomlins SA, Rao RC. Next generation sequencing of vitreoretinal lymphomas from small-volume intraocular liquid biopsies: new routes to targeted therapies [Internet]. Vol. 8. 2017.

32. Tan WJ, Wang MM, Castagnoli PR, Tang T, Chan ASY, Lim TS. Single B-Cell Genomic Analyses Differentiate Vitreoretinal Lymphoma from Chronic Inflammation. Ophthalmology. 2021 Jul 1;128(7):1079–90.
33. Péer J, Hochberg FH, Foster CS. Clinical review: Treatment of vitreoretinal lymphoma. Vol. 17, Ocular Immunology and Inflammation. 2009. p. 299–306.
34. Smith JR, Rosenbaum JT, Wilson DJ, Doolittle ND, Siegal T, Neuwelt EA, et al. Role of intravitreal methotrexate in the management of primary central nervous system lymphoma with ocular involvement. Ophthalmology. 2002 Sep;109(9):1709–16.
35. Frenkel S, Hendler K, Siegal T, Shalom E, Pe'er J. Intravitreal methotrexate for treating vitreoretinal lymphoma: 10 years of experience. Br J Ophthalmol. 2008 Mar;92(3):383–8.
36. Hashida N, Ohguro N, Nishida K. Efficacy and Complications of Intravitreal Rituximab Injection for Treating Primary Vitreoretinal Lymphoma. Transl Vis Sci Technol. 2012 Oct;1(3):1.
37. Cheah CY, Milgrom S, Chihara D, Gombos DS, Pinnix CC, Dabaja BS, et al. Intensive chemoimmunotherapy and bilateral globe irradiation as initial therapy for primary intraocular lymphoma. Neuro Oncol. 2016 Apr 1;18(4):575–81.
38. Kaburaki T, Taoka K, Matsuda J, Yamashita H, Matsuda I, Tsuji H, et al. Combined intravitreal methotrexate and immunochemotherapy followed by reduced-dose whole-brain radiotherapy for newly diagnosed B-cell primary intraocular lymphoma. Br J Haematol. 2017 Oct 1;179(2):246–55.
39. Castellino A, Pulido JS, Johnston PB, Ristow KM, Nora Bennani N, Inwards DJ, et al. Role of systemic high-dose methotrexate and combined approaches in the management of vitreoretinal lymphoma: A single center experience 1990-2018. Am J Hematol. 2019 Mar 1;94(3):291–8.
40. Soussain C, Choquet S, Fourme E, Delgadillo D, Bouabdallah K, Ghesquières H, et al. Intensive chemotherapy with thiotepa, busulfan and cyclophosphamide and hematopoietic stem cell rescue in relapsed or refractory primary central nervous system lymphoma and intraocular lymphoma: A retrospective study of 79 cases. Haematologica. 2012 Nov 1;97(11):1751–6.
41. Soussain C, Suzan F, Hoang-Xuan K, Cassoux N, Levy V, Azar N, et al. Results of intensive chemotherapy followed by hematopoietic stem-cell rescue in 22 patients with refractory or recurrent primary CNS lymphoma or intraocular lymphoma. J Clin Oncol. 2001 Feb 1;19(3):742–9.
42. Ferreri AJM, Cwynarski K, Pulczynski E, Ponzoni M, Deckert M, Politi LS, et al. Chemoimmunotherapy with methotrexate, cytarabine, thiotepa, and rituximab (MATRix regimen) in patients with primary CNS lymphoma: Results of the first randomisation of the International Extranodal Lymphoma Study Group-32 (IELSG32) phase 2 trial. Lancet Haematol. 2016 May 1;3(5):e217–27.
43. Hormigo A, Abrey L, Heinemann MH, DeAngelis LM. Ocular presentation of primary central nervous system lymphoma: Diagnosis and treatment. Vol. 126, British Journal of Haematology. 2004. p. 202–8.
44. Klimova A, Heissigerova J, Rihova E, Brichova M, Pytlik R, Spicka I, et al. Combined treatment of primary vitreoretinal lymphomas significantly prolongs the time to first relapse. British Journal of Ophthalmology. 2018 Nov 1;102(11):1579–85.
45. Cimino L, Coassin M, Chan CC, Marchi S, Belpoliti M, Fanti A, et al. Vitreoretinal lymphomas misdiagnosed as uveitis: Lessons learned from a case series. Indian J Ophthalmol. 2016 May 1;64(5):369–75.

46. Dalvin LA, Lim LAS, Ancona-Lezama D, Mazloumi M, Chang M, Porcu P, et al. Clinical features predictive of survival in patients with vitreoretinal lymphoma: Analysis of 70 patients at a single ocular oncology center. Asia-Pacific Journal of Ophthalmology. 2020;9(2):110–6.
47. Zicarelli F, Staurenghi G, Invernizzi A. Anterior Segment Optical Coherence Tomography (AS-OCT) Visualization of Anterior Vitritis. Vol. 31, Ocular Immunology and Inflammation. Taylor and Francis Ltd.; 2023. p. 1101–2.
48. Invernizzi A, Marchi S, Aldigeri R, Mastrofilippo V, Viscogliosi F, Soldani A, et al. Objective Quantification of Anterior Chamber Inflammation: Measuring Cells and Flare by Anterior Segment Optical Coherence Tomography. Ophthalmology. 2017 Nov 1;124(11):1670–7.
49. Keane PA, Karampelas M, Sim DA, Sadda SR, Tufail A, Sen HN, et al. Objective measurement of vitreous inflammation using optical coherence tomography. Ophthalmology. 2014;121(9):1706–14.
50. Zicarelli F, Ometto G, Montesano G, Motta S, De Simone L, Cimino L, et al. Objective Quantification of Posterior Segment Inflammation: Measuring Vitreous Cells and Haze Using Optical Coherence Tomography. Am J Ophthalmol. 2023 Jan 1;245:134–44.
51. Gozzi F, Bertolini M, Gentile P, Verzellesi L, Trojani V, De Simone L, et al. Artificial Intelligence-Assisted Processing of Anterior Segment OCT Images in the Diagnosis of Vitreoretinal Lymphoma. Diagnostics. 2023 Jul 1;13(14).
52. Park YG, Park WK, Kim RY, Kim M, Park YH. Serial changes in the aqueous IL-10 level after intravitreal methotrexate injection as an indicator of primary vitreoretinal lymphoma recurrence. Sci Rep. 2020 Dec 1;10(1).
53. Demirci H, Rao RC, Elner VM, Demirci FY, Axenov L, Betz B, et al. Aqueous Humor-Derived MYD88 L265P Mutation Analysis in Vitreoretinal Lymphoma: A Potential Less Invasive Method for Diagnosis and Treatment Response Assessment. Ophthalmol Retina. 2023 Feb;7(2):189–95.
54. Jensen LJ, Kim D, Elgeti T, Steffen IG, Schaafs LA, Hamm B, Nagel SN. Enhancing the Stability of CT Radiomics across Different Volume of Interest Sizes Using Parametric Feature Maps: A Phantom Study. Eur. Radiol. Exp. 2022, 6, 43.
55. Vallières M, Freeman CR, Skamene SR, El Naqa I. A Radiomics Model from Joint FDG-PET and MRI Texture Features for the Prediction of Lung Metastases in Soft-Tissue Sarcomas of the Extremities. Phys. Med. Biol. 2015, 60, 5471–5496.
56. Vallières M, Kay-Rivest E, Perrin LJ, Liem X, Furstoss C, Aerts HJWL, Khaouam N, Nguyen-Tan PF, Wang CS, Sultanem K, Seuntjens J, El Naqa I. Radiomics strategies for risk assessment of tumour failure in head-and-neck cancer. Sci Rep. 2017 Aug 31;7(1):10117.
57. Zhou H, Vallières M, Bai HX, Su C, Tang H, Oldridge D, Zhang Z, Xiao B, Liao W, Tao Y, Zhou J, Zhang P, Yang L. MRI features predict survival and molecular markers in diffuse lower-grade gliomas. Neuro Oncol. 2017 Jun 1;19(6):862-870.
58. Pedregosa, F.; Varoquaux, G.; Gramfort, A.; Michel, V.; Thirion, B.; Grisel, O.; Blondel, M.; Prettenhofer, P.; Weiss, R.; Dubourg, V.; et al. Scikit-Learn: Machine Learning in Python. J. Mach. Learn. Res. 2011, 12, 2825–2830.
59. Liu S, Jiang T, Gu J, Zhou X, Chen W, Ping B, et al. Prognosis, Risk Factors, and Clinical Features of Intraocular Recurrence in Primary Vitreoretinal Lymphoma. Ophthalmol Retina. 2024 Apr 1;8(4):317–24.

60. Abrey LE, Batchelor TT, Ferreri AJM, Gospodarowicz M, Pulczynski EJ, Zucca E, et al. Report of an international workshop to standardize baseline evaluation and response criteria for primary CNS lymphoma. Vol. 23, Journal of Clinical Oncology. 2005. p. 5034–43.
61. Jensen LJ, Kim D, Elgeti T, Steffen IG, Schaafs L-A, Hamm B & Nagel SN (2022): Enhancing the stability of CT radiomics across different volume of interest sizes using parametric feature maps: a phantom study. Eur Radiol Exp 6: 43.
62. Grueschow M, Stenz N, Thörn H, et al. (2021): Responsivity of the locus coeruleus. Nat Commun 1–17.
63. Nibid L, Greco C, Cordelli E, et al. (2023): Deep pathomics : A new image-based tool for predicting response to treatment in stage III non-small cell lung cancer. PLoS One 1–24.
64. Lundberg SM, Erion G, Chen H, et al. (2020): From local explanations to global understanding with explainable AI for trees. Nat Mach Intell 2: 56–67.
65. Lundberg SM, Erion GG & Lee S (2018): Consistent Individualized Feature Attribution for Tree Ensembles. arXiv.
66. Lundberg SM & Lee SI (2017): A unified approach to interpreting model predictions. Adv Neural Inf Process Syst 2017-Decem: 4766–4775.
67. Sebag, J. Vitreous and Vision Degrading Myodesopsia. Prog. Retin. Eye Res. 2020, 79, 100847.
68. Ruminski D, Sebag J, Toledo RD, Jiménez-Villar A, Nowak JK, Manzanera S, Artal P, Grulkowski I. Volumetric Optical Imaging and Quantitative Analysis of Age-Related Changes in Anterior Human Vitreous. Invest Ophthalmol Vis Sci. 2021 Apr 1;62(4):31.
69. Spaide RF, Valmaggia P, Maloca PM, Scholl HPN, Otto TP, Caujolle S. Imaging the vitreous with a novel boosted optical coherence tomography technique: Vitreous Degeneration and Cisterns. Retina. 2022 Aug 1;42(8):1433-1441.
70. Prasanna P, Bobba V, Figueiredo N, Sevgi DD, Lu C, Braman N, Alilou M, Sharma S, Srivastava SK, Madabhushi A, Ehlers JP. Radiomics-based assessment of ultra-widefield leakage patterns and vessel network architecture in the PERMEATE study: insights into treatment durability. Br J Ophthalmol. 2021 Aug;105(8):1155-1160.
71. Afarid M, Mohsenipoor N, Parsaei H, Amirmoezzi Y, Ghofrani-Jahromi M, Jafari P, Mohsenipour A, Sanie-Jahromi F. Assessment of macular findings by OCT angiography in patients without clinical signs of diabetic retinopathy: radiomics features for early screening of diabetic retinopathy. BMC Ophthalmol. 2022 Jun 27;22(1):281.
72. Lambin P, Rios-Velazquez E, Leijenaar R, Carvalho S, van Stiphout RG, Granton P, Zegers CM, Gillies R, Boellard R, Dekker A, Aerts HJ. Radiomics: extracting more information from medical images using advanced feature analysis. Eur J Cancer. 2012 Mar;48(4):441-6.
73. van Griethuysen JJM, Fedorov A, Parmar C, Hosny A, Aucoin N, Narayan V, Beets-Tan RGH, Fillion-Robin JC, Pieper S, Aerts HJWL. Computational Radiomics System to Decode the Radiographic Phenotype. Cancer Res. 2017 Nov 1;77(21):e104-e107.
74. Yoo TK, Choi JY, Kim HK. Feasibility study to improve deep learning in OCT diagnosis of rare retinal diseases with few-shot classification. Med Biol Eng Comput. 2021 Feb;59(2):401-415.
75. Tafuri B, Lombardi A, Nigro S, Urso D, Monaco A, Pantaleo E, Diacono D, De Blasi R, Bellotti R, Tangaro S, Logroscino G. The impact of harmonization on radiomic features in Parkinson's disease and healthy controls: A multicenter study. Front Neurosci. 2022 Oct 10;16:1012287.

76. Bertolini M, Trojani V, Botti A, Cucurachi N, Galaverni M, Cozzi S, Borghetti P, La Mattina S, Pastorello E, Avanzo M, Revelant A, Sepulcri M, Paronetto C, Ursino S, Malfatti G, Giaj-Levra N, Falcinelli L, Iotti C, Iori M, Ciammella P. Novel Harmonization Method for Multi-Centric Radiomic Studies in Non-Small Cell Lung Cancer. Curr Oncol. 2022 Jul 22;29(8):5179-5194.
77. Orlhac F, Eertink JJ, Cottereau AS, Zijlstra JM, Thieblemont C, Meignan M, Boellaard R, Buvat I. A Guide to ComBat Harmonization of Imaging Biomarkers in Multicenter Studies. J Nucl Med. 2022 Feb;63(2):172-179.
78. Soliman MAS, Kelahan LC, Magnetta M, Savas H, Agrawal R, Avery RJ, Aouad P, Liu B, Xue Y, Chae YK, Salem R, Benson AB, Yaghmai V, Velichko YS. A Framework for Harmonization of Radiomics Data for Multicenter Studies and Clinical Trials. JCO Clin Cancer Inform. 2022 Nov;6:e2200023.
79. Gillies RJ, Kinahan PE, Hricak H. Radiomics: Images Are More than Pictures, They Are Data. Radiology. 2016 Feb;278(2):563-77.